Title
SCATTERING OF 310-MSV POSITIVE PIONS BY PROTONS: EXPERIMENTS AND ANALYSIS.

Author
Rogers, Ernest H.

Publication Date
1962-03-19

UCRL 10127

cy 2

University of California

Ernest O. Lawrence Radiation Laboratory

ERNEST ROGERS (Ph.D. THESIS)

MARCH, 19[illegible] 1962

Berkeley, California

DISCLAIMER

TECHNICAL INFORMATION DIVISION

Lawrence Radiation Laboratory

Berkeley

Assigned to INFORMATION DIVISION

Route to	Noted

Please return this document to the Information Division. Do not send it to the next person on the list.

Please do not remove this page.

UCRL-10127
UC-34 Physics
TID-4500 (17th Ed.)

UNIVERSITY OF CALIFORNIA

Lawrence Radiation Laboratory
Berkeley, California

Contract No. W-7405-eng-48

SCATTERING OF 310-MEV POSITIVE PIONS BY PROTONS: EXPERIMENTS AND ANALYSIS

Ernest H. Rogers

(Ph. D. Thesis)

March 19, 1962

SCATTERING OF 310-MEV POSITIVE PIONS BY PROTONS: EXPERIMENTS AND ANALYSIS

Contents

SCATTERING OF 310-MEV POSITIVE PIONS BY PROTONS: EXPERIMENTS AND ANALYSIS

Ernest H. Rogers

Lawrence Radiation Laboratory
University of California
Berkeley, California

March 19, 1962

ABSTRACT

The differential cross section for elastic scattering of 310-Mev positive pions on protons has been measured at 23 angles between 14 deg and 165 deg in the center-of-mass system. The fractional rms errors were typically 3%. A liquid hydrogen target was bombarded by a beam of 2×10^6 pions/sec. The scattered pions were detected by a counter telescope. The data at small angles clearly show constructive interference between nuclear and Coulomb interactions. A total cross section of 60.0 ± 1.4 mb was measured by attenuation.

These data were combined with data on the polarization of the recoil proton, which were taken simultaneously with the cross-section measurements, and a phase-shift analysis was made. This analysis was hampered by the small angular region covered by the polarization data (114 deg to 145 deg), but even this limited amount of information about the polarization proved extremely valuable. It was impossible to obtain an adequate fit to the data in terms of only S- and P-wave phase shifts. However, a very satisfactory fit was obtained when D waves were also included. Moreover, this solution was unique. Only one set of SPD-wave phase shifts agreed with the data. This set was of the Fermi type. When F waves were also included in the analysis, the fit to the data was not improved significantly. However, the errors on the S-, P-, and D-wave phase shifts increased from about 1/2 deg to around 2-1/2 deg, and additional sets of phase shifts that fit the data arose. The S-, P-, and D-wave phase shifts differ considerably among the various sets, even though the F-wave phase shifts are quite small. Most of these sets may be discarded by theoretical arguments, but one is left with at least two possible Fermi-type SPDF solutions.

I. INTRODUCTION

The investigation of the pion-nucleon interaction is of fundamental importance to the progress of nuclear physics. For example, the nucleus is thought to be held together by forces arising mainly from the exchange of pions between various nucleons. The investigation of the scattering of pions on nucleons is the most direct method of examining the pion-nucleon interaction experimentally. Any satisfactory theory of the pion-nucleon interaction, or any more comprehensive theory of strong interactions, must encompass this data. At present neither theory nor experiment seems to be satisfactory. The purpose of this work was to give a more accurate experimental description of pion-nucleon scattering in order to provide a more stringent test of present and future theories, and perhaps to suggest lines of future theoretical development.

Pion-nucleon scattering experiments are usually analyzed in terms of phase shifts. Each phase shift describes the scattering for a particular quantum-mechanical state of orbital angular momentum $\ell\hbar$, and total angular momentum $J\hbar$, of the pion-nucleon system. These parameters provide the traditional meeting ground between theory and experiment. The motivation for this approach comes from the short-range character of the pion-nucleon force, which implies that the first few angular-momentum states dominate the interaction. For example, viewing the scattering classically, if the incident pion energy is 300 Mev, an impact parameter of 1 pion Compton wavelength corresponds to $\ell = 2$. If, as we expect, 1 pion Compton wavelength is a reasonable estimate of the range of the interaction, then the main contribution to the scattering will come from states of $\ell \leq 2$. The contribution from higher-order terms (larger ℓ value) will become progressively smaller quite rapidly. Therefore, one expects to describe the scattering at this energy fairly accurately in terms of only S-, and P-, or S-P- and D-wave phase shifts. S, P, D etc., represent states of $\ell = 0, 1, 2$, etc., in the usual way. There are two possible values of J for each value of ℓ, namely $J = |\ell \pm 1/2|$. In our phase-shift notation, the firstsubscript is twice the isotopic spin. The isotopic spin is always 3/2 for $\pi^+ p$ scattering, but may be either 1/2 or 3/2 for $\pi^- p$ scattering. The second subscript is 2J (e.g. $P_{3,3}$ is the phase shift

for $\ell = 1$, $J = 3/2$). It is also clear from this classical analogy that higher-order phase shifts are expected to become important when the scattering energy is increased. In order to obtain phase shifts from experimental data, one has to neglect the small phase shifts, i.e., set all phase shifts equal to zero for ℓ greater than some value ℓ_{max}. The nonzero phase shifts are then required to fit the experimental data. ℓ_{max} must be determined experimentally. We assume that the values of the large phase shifts obtained from the analysis are not distorted by neglecting the small phase shifts. The earlier analyses of positive pion-proton scattering have generally been made in terms of only S- and P-wave phase shifts ($\ell_{max} = 1$). It was possible to obtain acceptable fits to the experimenta data in terms of S- and P-waves, and the data were not sufficiently accurate to obtain meaningful results if D waves were included ($\ell_{max} = 2$). The data consisted entirely of differential and total cross-section measurements. Attempts to obtain phase shifts from cross-section data were hindered by ambiguities. These ambiguities are of several types, but all give rise to the same situation. That is, they give a prescription for taking a given set of phase shifts and producing another set which yields the same, or nearly the same, differential cross section as the first. Therefore, there are several sets of phase shifts that fit the differential cross section equally well. However, Fermi pointed out that in general these various sets of phase shifts predict different values of the polarization of the recoil proton.[1] So, in principle, these ambibuities could be resolved by measuring the polarization, but pion-beam fluxes were too low to make this experiment feasible. The various ambiguities are: (a) the Yang, in which the sign of $(P_{3,3}-P_{3,1})$ is reversed;[2] (b) a similar D-wave ambiguity first pointed out by Clementel and Villi;[3] (c) the Minami ambiguity, in which all phase shifts of the same J and different ℓ are interchanged;[4] (d) the sign ambiguity, in which the signs of all the phase shifts are reversed.[2] The Minami ambiguity has been resolved by comparing the energy dependence of the phase shifts at low energy with general theoretical predictions.[2,5] Fermi's choice of P-wave phase shifts has been generally accepted, mostly because they are strongly favored from a theoretical standpoint. There is also some indication that the Yang-type solutions may not agree

with the requirements of the dispersion relations for the spin-flip forward-scattering amplitude.[6] The sign ambiguity was resolved by observing the interference between nuclear scattering and Coulomb scattering.[7] The knowledge about the phase shifts from earlier experiments was then:

$P_{3,3}$ is large and postive. It rises rapidly and passes through resonance (90 deg) at about 190 Mev.

$S_{3,1}$ is negative. Its magnitude, which increases with energy, was not well known above the resonance, where the inclusion of small D-wave phase shifts in the analysis can affect its value substantially.

$P_{3,1}$ is small. Its sign was not reliably determined.

$D_{3,3}$ and $D_{3,5}$ were virtually undetermined. The D-wave phase shifts were thought to be less than 15 deg, because the data could be adequately fitted in terms of only S and P waves. The most striking feature of this scattering is the resonance in the $P_{3,3}$ state. This state dominates the cross-section data to such an extent that it has been difficult to determine the smaller phase shifts accurately. However, the polarization of the recoil proton, which comes from interference between phase shifts, is more sensitive to the values of the small phase shifts.

In order to resolve these various ambiguities experimentally, and to obtain accurate values for the smaller phase shifts, an effort to measure the polarization of the recoil proton was clearly called for. However, in order to make use of the polarization data, it was also necessary to measure the differential cross section more accurately than previous experimenters have done. For example, when the data of Mukhin et al., which were the best cross-section data before our experiment, were analyzed, several ambiguous sets of phase shifts were obtained.[8] Each set predicted quite different values for the polarization. However, the accuracy of these predictions was quite poor. In general, almost any value of the polarization was consistent with the cross-section data for all types of solutions.

For these reasons, we have made some measurements of the polarization of the recoil proton and a relatively accurate measurement of the differential cross section of π^+-p scattering at an incident-pion

kinetic energy of 310 Mev in the laboratory system. The emphasis was placed on obtaining maximum accuracy and reliability at this one energy, rather than on obtaining data at several energies. This scattering energy was chosen for several reasons. The pion flux at 310 Mev was near to the maximum obtainable from the 184-in. cyclotron. A small increase in energy would have brought an appreciable loss in pion flux, which would have seriously hampered the polarization experiment. A reduction in the scattering energy would have limited the angular region over which polarization data could be obtained even further, because this limit results from the fact that polarization could be measured only when proton energy was greater than 140 Mev.

At this energy, inelastic scattering is negligible. The cross section for inelastic scattering is about 1/2 mb, compared with 60 mb for elastic. This makes the measurements easier and also simplifies the phase-shift analysis, because the phase shifts are restricted to real quantities in the case of pure elastic scattering.

II. PION BEAM

The relatively low flux of previous pion beams was the major factor both in limiting the accuracy of earlier cross-section experiments, and in discouraging any attempt to measure the polarization. Therefore, in order to carry out the proposed experiments, it was necessary to develop a very intense pion beam. In addition to high intensity, there were certain other restraints to be imposed upon this beam. In order that the angle of scattering be well defined, the divergence and the size of the beam had to be small at the hydrogen target, where the scattering occurred. The energy spread of the beam had to be rather small so that the scattering occurred at a well-defined energy. The contamination (particles other than pions in the beam) had to be minimized, and the region around the hydrogen target had to be sufficiently free of stray radiation so that the level of background events in the counters was tolerable. The beam which was developed met all these requirements fairly well. The intensity was 2×10^6 pions/sec, or about 10^3 greater than the beams developed by previous experimenters. The beam covered an area about 2 in. in diameter at the hydrogen target, and contained only a small contamination of 4% muons and 1/4% positrons. The energy of the beam was 310±3 Mev at the center of hydrogen target, and the rms energy spread was ±9 Mev. A description of the apparatus used to produce this beam is given in the next section. A modification of this system, in which intensity was sacrificed in order to obtain smaller energy spread, beam size, and beam divergence, is described in Section IV-B.

A. Magnet System

A scale drawing of the apparatus used to make the positive-pion beam is shown in Fig. II-1. The external proton beam of the Berkeley 184-in. cyclotron was used to produce the pions. The intensity of the external beam is only a few percent of that of the internal beam, but the increased solid angle, increased effective target thickness, and the increase in yield due to 0-deg production that one gains by using an external target more than make up for this loss in proton flux. The proton beam is steered through the main cyclotron shielding and

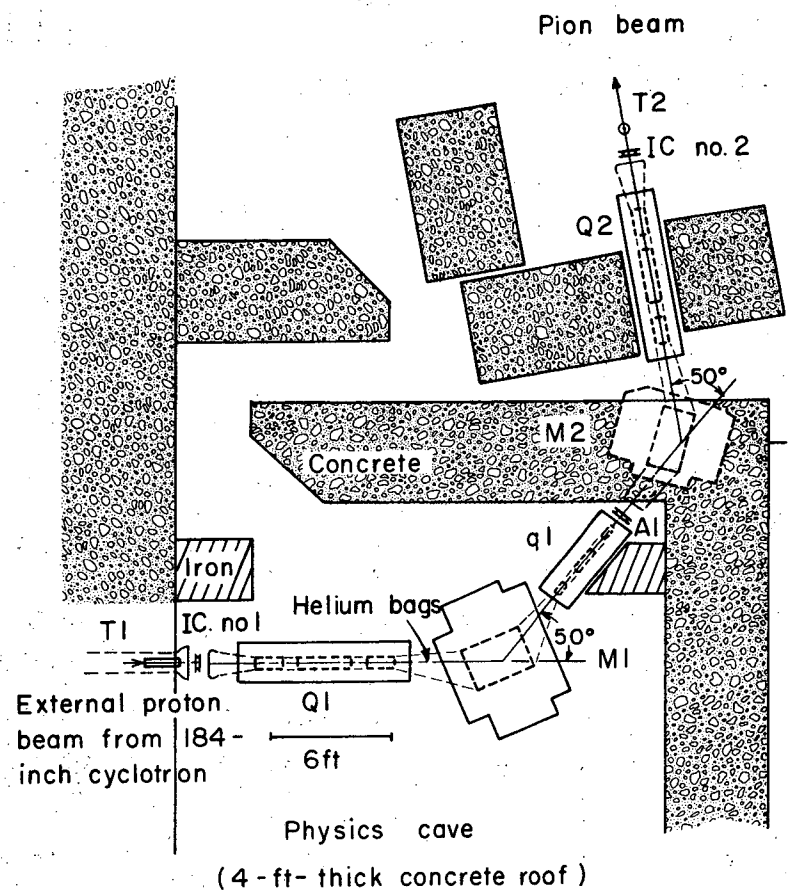

Fig. II-1. Scale drawing (plan view) of pion spectrograph No. 1. A description of the components is given in Table III-1.

focused on a polyethlene target T1 in the physics cave. The external beam at this point fell in an area about 2 in. square and had a maximum intensity of about 2×10^{11} protons/sec. Its energy was 745 Mev with an rms spread of ±8 Mev. The position and size of the proton beam were determined by exposing x-ray film in the beam.

The pions were produced by the interaction of the proton beam with a polyethlene (CH_2) target T1. The choice of this material for the production target was, fortunately, very simple, because hydrogen was particularly valuable. The reaction $p + p \rightarrow \pi^+ + d$ has a relatively high cross section, especially for pions produced in the forward direction.[1] Because there are only two particles in the final state, the pions have a unique energy at any given angle, for a particular incident-proton energy. The really fortunate fact is that if one looks at the pions produced in the forward direction from a thick target, all the pions produced by the $p + p \rightarrow \pi^+ + d$ reaction are nearly monoenergetic upon leaving the target. This is because the mesons created in the front part of the target and slowed down in the target have approximately the same energy as the mesons produced by the moderated protons at the rear of the target. Of course it is very important that the target length be chosen to yield mesons of the same energy as the magnet system selects. In this case, the optimum target thickness turned out to be 19 in. Pions were produced by other reactions in the target, but in these reactions the pions were produced over a wide range of energy, of which we accepted only a small slice.[9,10] Therefore, this type of production was less important.

The magnet system selected positive mesons of the desired momentum from the debris at T1 and focused them on the hydrogen target T2. In order to gather as many useful pions as possible into the system, a quadrupole focusing magnet Q1 was placed close to the production target. Useful pions that entered the first quadrupole were focused at the center of q1. A "triplet"-type quadrupole was used at Q1, because a doublet type yields a lower effective solid angle for asymmetrical object and image distances. In this system, a doublet quadrupole of the same physical aperture as the triplet would have had only 1/2 the effective aperture. The beam was deflected 50 deg by

magnet M1, which introduced a dispersion according to

$$\Delta\theta = - \frac{\Delta P}{P} \; 2 \tan \frac{\theta}{2},$$

where P is the particle momentum for which the system is adjusted, θ is the bending angle at the deflecting magnet, and $\Delta\theta$ is the deviation in bending angle of a particle whose momentum is P+ΔP. This caused a momentum dispersion of about 1% per in. at q1; i.e., for a point source at T1, and therefore a point image at q1, all positive particles whose momentum was within ±2% of the central momentum would enter the 4-in. aperture of q1, and all those whose momentum was more than 2% off would fall outside this aperture. The finite size of object and image smeared this selection somewhat, allowing a few particles whose momentum was off by 3% and preventing some whose momentum was off by only 1% to enter q1. The beam then passed through a second deflecting magnet M2 and quadrupole lens Q2, which were placed symmetrically with Q1 and M1 about q1. The second 8-in. quadrupole Q2 brought the beam to a second focus at T2.

Because of the symmetry of this double spectrograph, the image at T2 was dispersion-free, and the size of the pion beam at T2 was about the same as the size of the proton beam at T1, i.e., about 2 in. in diameter. The 4-in.-diameter quadrupole q1 acted as a field lens. The object and image planes of this lens were the exit end of Q1 and the entrance end of Q2, respectively. As q1 was placed right at the first focus of the beam, this magnet could be turned on or off without affecting the position of the second focus at T2. The result of turning off q1 was to cause some of the beam that passed through q1 to miss the entrance of Q2. With this field lens turned on, almost all of the particles that entered the aperture of q1 also entered Q2. The gain in flux at the final focus caused by the field lens was about 70%. However, because the particles that were saved by the field lens were either produced off the axis or off the central momentum, the image size at the final focus was increased somewhat by the presence of the field lens. Finally, it is clear that a field lens must always be of the triplet type, because unit magnification is required in both planes to focus the rear of one quadrupole onto the front of another.

A 2-in. carbon absorber A1 was placed just after q1. Because the beam is of monomomentum after passing through q1, the carbon absorber stopped the proton component of the beam, as well as deuterons, α particles, etc., while slowing the mesons only slightly. Just before this absorber there were roughly equal numbers of pions and protons in the beam. Because this absorber was very near to the first focus, it did not increase the size of the beam at the second focus appreciably; however, a few percent of the pions were scattered out of the beam. The entire beam channel from the production target to the final focus was enclosed by plastic bags filled with helium. The purpose of the helium was to reduce multiple Coulomb scattering of the pion beam, because this multiple scattering tended to smear out the size of the beam at the final focus. In fact, the area of the beam was increased fourfold when the helium bags were removed. The helium reduced the effect of the multiple scattering to a point at which it was unimportant compared with the natural image size, so that the use of a vacuum system to further reduce multiple scattering was not necessary.

The production and momentum selection of the beam took place inside the physics cave so that the proton beam that passed through T1 and all the particles produced at T1, except the pions in the beam, would be contained in the cave. Therefore, the area around the second focus, where the experiments took place, was relatively free of background.

Proper currents for the focusing and deflecting magnets were calculated approximately and optimized by the suspended-wire method. This method makes use of the fact that a current-carrying wire assumes the same orbit as a charged particle of momentum P, if the tension in the wire, T, and the wire current I are chosen according to

$$I\,(\text{in amps}) = 2.94\,T\,(\text{in grams})/P(\text{in Mev/c}).$$

By this method, the energy of the pion beam was fixed with an accuracy of better than 1%, and the positions of the focuses were determined to within a few inches. The alignment of the entire system was checked by passing the wire through the system from T1 to T2 with the quadrupoles turned off and seeing that the wire passed through the centers of all the

quadrupoles. Finally the system was checked by measuring the acceptance $\Delta\Omega\ \Delta P/P$ of the system, using particles produced at T1, and comparing this value with predicted values. The $\Delta\Omega$ is the effective solid angle and $\Delta P/P$ is the effective fractional momentum bite for particles produced at T1 to arrive at T2. The method used to measure the acceptance is described in another paper.[11] The result for this beam was

$$\Delta\Omega\ \Delta P/P = 1.3 \times 10^{-4}\ \text{sr}.$$

The pion beam exhibits a structure in time that reflects the acceleration characteristics of the 184-in. cyclotron. The repetition rate of 64 acceleration cycles per second gives 64 groups of pions per second, each of which is composed of fine-structure pulses of width 5×10^{-9} sec and spaced 52×10^{-9} sec apart, corresponding to the final accelerating radio frequency of 19.2 Mc/sec. A schematic drawing of the time structure of the beam is given in Fig. II-4. The duration of the coarse groups was about 35 μ/sec, therefore each group was composed of about 700 rf pulses. The beam was contained in 40,000 rf pulses/sec., so there were, on the average, 50 pions in each pulse. Pions in the same rf pulse could not be resolved electronically, so it was impossible to count the beam with scintillation counters. Therefore the pion beam was monitored by an argon-filled ionization chamber. The chamber was similar to one described by Owen Chamberlain, Emilio Segrè, and Clyde Wiegand.[12] The ion-chamber current was measured by a standard electrometer and displayed on a recorder. The absolute conversion of ion-chamber current to meson flux was made by using the calibration by Chamberlain et al. It was necessary to assume that the average energy loss per ion pair formed was the same for 310-Mev pions as it was for 340-Mev protons. The relative energy loss in these two cases was taken from the tables of Rich and Madey.[13] The ion chamber was found to give results independent of the applied voltage over a wide range in voltage, and its drift was negligible (i.e., the current collected when the pion beam was turned off was $< 0.1\%$ of the current due to the beam).

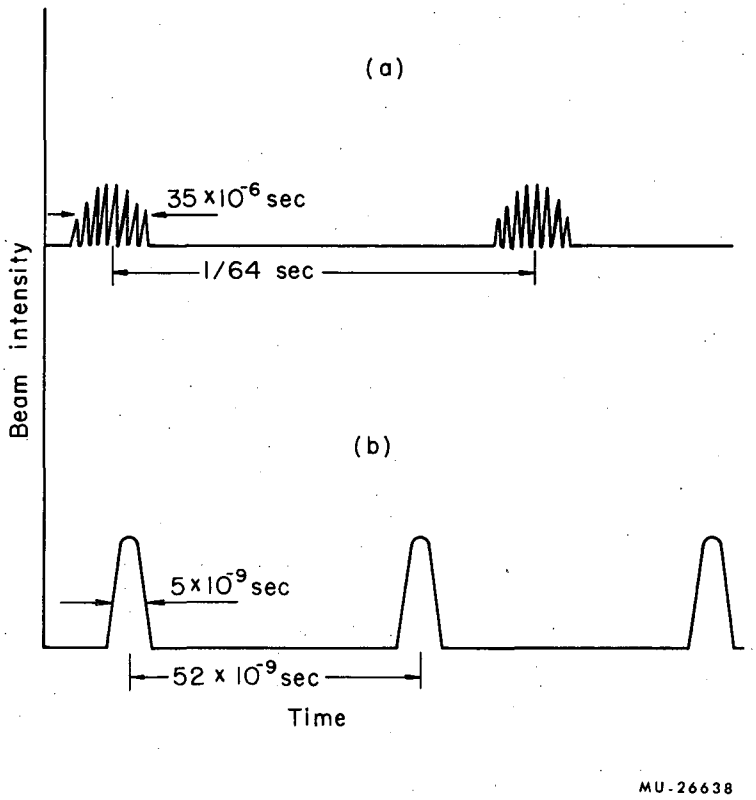

Fig. II-4. Time structure of the pion beam, showing (a) timing of the coarse groups, and (b) rf structure of the coarse groups.

B. Contamination

The pion beam contained a small percentage of muons and a negligibly small fraction of positrons. It was necessary to correct the ion-chamber current for this contamination in order to obtain the true meson flux. There were two principal sources of muon contamination; one was the region of the production target T1 and the other was the decay of pions in that section of the beam just before the ion chamber. The muons arising from these two sources had very different energy and spatial distributions and therefore were examined separately.

The muons produced near the production target (T1) arrived at the second focus (T2) with a definite momentum of 430±4 Mev/c, since they had been analyzed by the spectrometer. These muons had a greater range than the pions of that momentum; therefore, they stood out as a tail on the pion range curve. Figures II-2 and II-3 show a range curve of the second beam, with the muon tail clearly visible. This curve was obtained with a setup similar to that shown in Fig. V-1, except the hydrogen target was removed and counter S3 was placed 13 in. downbeam from S3. A variable-thickness copper absorber was centered between counters S8 and S3. The fraction of transmitted pions S7, C1, S8, S3)/(S7, C1, S8) was measured as a function of absorber thickness. An absorber thickness of 190 g/cm^2 appeared to be greater than the range of virtually all the pions and less than the range of most muons. The muons visible at this range comprise 2.8% of the incident beam. However, a calculation based on a paper by Sternheimer[14] indicated that, for this geometry and absorber thickness, 28% of the muons were scattered out of the back-up counter (S3) by multiple Coulomb scattering. Therefore, this muon contamination comprised 3.9% of the beam. The multiple-scattering correction was checked by redoing the range curve with the copper absorber moved 1 in. and 2 in. closer to the back-up counter. The apparent muon contamination rose to 3.3% and 3.6%, respectively; both are consistent with a true contamination of 3.9%.

About 40% of the pions in the beam decay into muons before they arrive at the hydrogen target. Some of these muons are counted in the ion chamber. The muons, which come from pions decaying before the first focus q1, must pass through the second spectrograph in order to

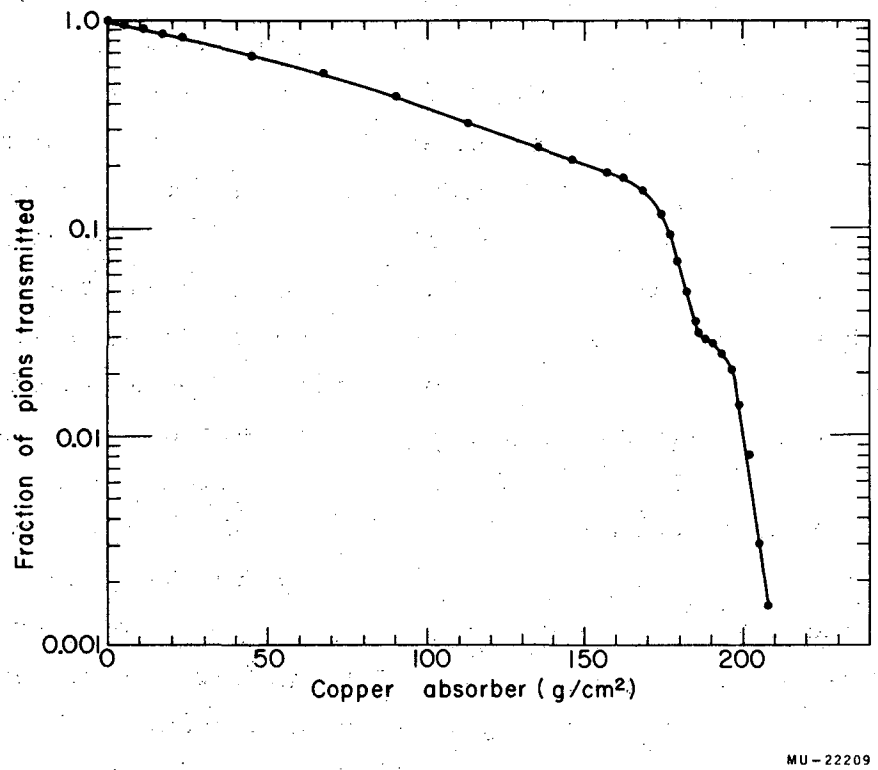

Fig. II-2. Pion beam range curve: semilog scale.

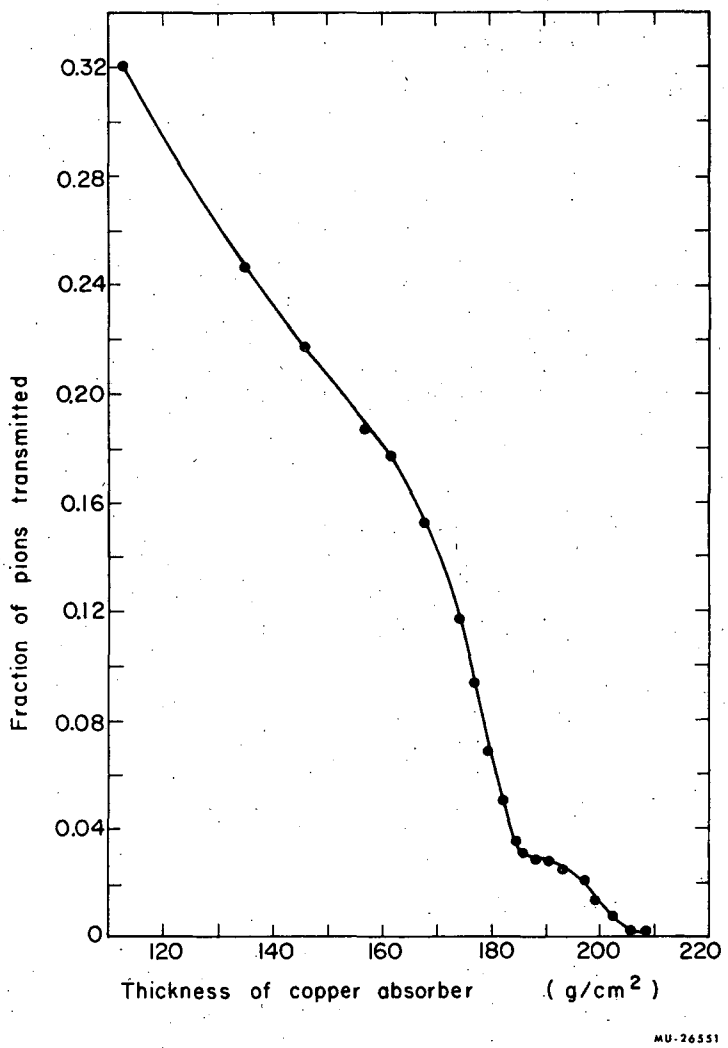

Fig. II-3. Tail of the pion-beam range curve: standard scale.

reach the ion chamber. They must have the proper momentum, and therefore, show up in the range curve in the same way as muons produced near the production target T1 do. As for the pions that decayed in the second half of the system, it was necessary to calculate what fraction of them would send muons into the ion chamber. The kinematics of the decay and the beam geometry were well known, so the calculation was straightforward. The probability P that a pion will decay in an increment of path length $\Delta\ell$ is

$$P = \Delta\ell / \tau_\pi \beta\gamma c,$$

where τ_π is the mean life of a pion at rest (2.55×10^{-8} sec), and β and γ are the usual relativistic functions of pion velocity in the laboratory. For pions in this beam the mean decay length is $\tau_\pi \beta\gamma c = 930$ in. One must also use the fact that the muons appear isotropically in the pion rest frame. Then in the laboratory system these muons fall inside a cone of half angle 5.3 deg with respect to the pion momentum vector, with most of the muons found near the edge of this cone. Therefore only pions that decay within a few feet of the ion chamber have an appreciable chance of yielding a muon that passes through the ion chamber. The result was that 6.1% of the particles passing through the ion chamber were muons of this kind. The momentum of these muons was uniformly distributed between 242 and 435 Mev/c, corresponding to a range in copper of 82 to 205 g/cm^2; therefore it was impossible to identify them on the range curve.

The number of positrons in the beam was expected to be small. They originate from pairs produced by neutral pions. A great many neutral pions were produced along with the positive pions, but their number decreased rapidly with increasing energy for energies greater than 350 Mev. The energy of a neutral pion had to be split four ways, between two positrons and two electrons; therefore, the relative probability of finding a 430-Mev positron was small. The fraction of positrons in the pion beam was measured by using a gas Cerenkov counter.[15] This counter had a threshold of $\beta = 0.99$; therefore, it detected only the positron component of the beam. The positron contamination was found to be 1/4% of the beam. This result was checked by taking a Bragg curve of the pion beam. Variable-thickness lead sheets were placed in front of the ion chamber, and the ion chamber

current was plotted as a function of absorber thickness. If there had been an appreciable positron contamination in the beam, a typical shower curve would have been observed. That is, the ion-chamber current due to positrons in the beam would have increased to about six times its initial value at 3/4 in. of lead, then dropped off, passing through its initial value at 2-1/2 in. of lead.[16] No such effect was observed; instead the ion-chamber current decreased smoothly through this range of absorber. These data showed that the positron contamination was definitely less than 1%. This Bragg curve was also a very sensitive method of showing that no protons had sneaked into the beam. The fact that the ionization loss of protons is greater by a factor of 3-1/3 than that for pions at the momentum of this beam, and the characteristic bump in the curve just before the end of the proton range, would have caused a small proton contamination (1% or greater) to stand out clearly on the Bragg curve.

III. DIFFERENTIAL CROSS-SECTION MEASUREMENTS

For sufficiently thin targets, the differential cross section $\frac{d\sigma}{d\Omega}(\theta)$ is defined as

$$\frac{d\sigma}{d\Omega}(\theta) = \frac{I(\theta)}{I_0 \Omega N},$$

where, for pion-proton scattering, I_0 is the number of pions incident on the target, and N is the thickness of the target in units of protons/cm^2; $I(\theta)$ is the number of pions scattered into a counter, which subtends a solid angle Ω as seen from the target, and lies at an angle θ with respect to the incident-beam direction. The method and results of differential cross-section measurements between 22.0 deg and 159.2 deg in the laboratory system are described in this section. A modified system, which allowed cross-section measurements to be made down to 10 deg in the laboratory frame, is described in Section IV.

A. Method and Apparatus

The objective of this experiment was to obtain data significantly more accurate than had been obtained previously, by utilizing the relatively high intensity of this pion beam. The most obvious advantage came from the large number of scattering events that could be observed. Whereas previous experiments obtained about a hundred events at each scattering angle, thousands were obtained in this experiment, and more scattering angles were examined. This resulted in a considerable gain in accuracy, because the statistical counting error is proportional to the square root of the number of events observed. However, in order for these smaller statistical errors to be meaningful, it was also necessary to reduce systematic errors in the apparatus proportionately. This was accomplished in two ways. First, the apparatus was designed so that the various corrections to the data were small. These corrections, due to telescope efficiency, plural scattering, finite target, and counter size, etc., could not be determined accurately. Therefore, to keep them from corrupting the data, it was necessary to make their effect small. Secondly, numerous checks of possible systematic errors were made, e.g., range curves of the scattered beam, repeating the data-taking at lower beam levels, etc. All this was possible only because of

the high incident flux, and would have been too time-consuming in earlier experiments.

Figure III-1 shows the setup used to obtain the major part of the data. Table III-I summarizes the specifications of the beam-forming and counting equipment. The incident pion beam I_0, was monitored by the ion chamber as described in Section II. Pions which scattered from the liquid hydrogen target were detected by the counter telescope. At some angles it was also possible to detect the recoil proton in coincidence with the scattered pion. The bulk of the data, referred to as run No. 1, were taken by using the high-intensity pion beam described in Section II; the polarization measurements (see Section VI) were made simultaneously with an independent counter system around the same hydrogen target. Some data were taken with the lower-intensity beam (beam No. 2) described in Section IV; these data are referred to as run No. 2.

The liquid hydrogen was contained in a stainless steel cylinder 5.51 in. in diam and 8.0 in. long. The walls of the cylinder were 0.005 in. thick, and its axis was oriented in the up-down direction, perpendicular to the plane of scattering. The target was connected to a liquid hydrogen reservoir which was vented to the atmosphere. The vacuum jacket had 0.125-in. aluminum walls with 3-in. diam and 0.015-in. thick Mylar windows for the entrance and exit of the beam. In order to find the effective target length, N, it was necessary to average the length in beam direction over distance from center target, using the beam profile as a weighting function. The effective length determined in this way was 4.82 in. For this purpose, the beam profile at the target position was taken accurately, and checked periodically during the experiment. This profile was measured by sweeping a counter telescope, consisting of two square scintillation counters 0.50 and 0.25 in. on a side, through the beam. The density of liquid hydrogen was taken to be 0.0702 g/cm^2, giving $N = 5.13 \times 10^{23}$ protons/cm^2.[17]

The pions scattered from the liquid hydrogen target were detected by a three-counter telescope S1, S2, C1. S2 was the defining counter. It was a 2.25-in. -diam scintillation counter at a distance of 68.25 in. from the center of the hydrogen target, corresponding to a solid angle

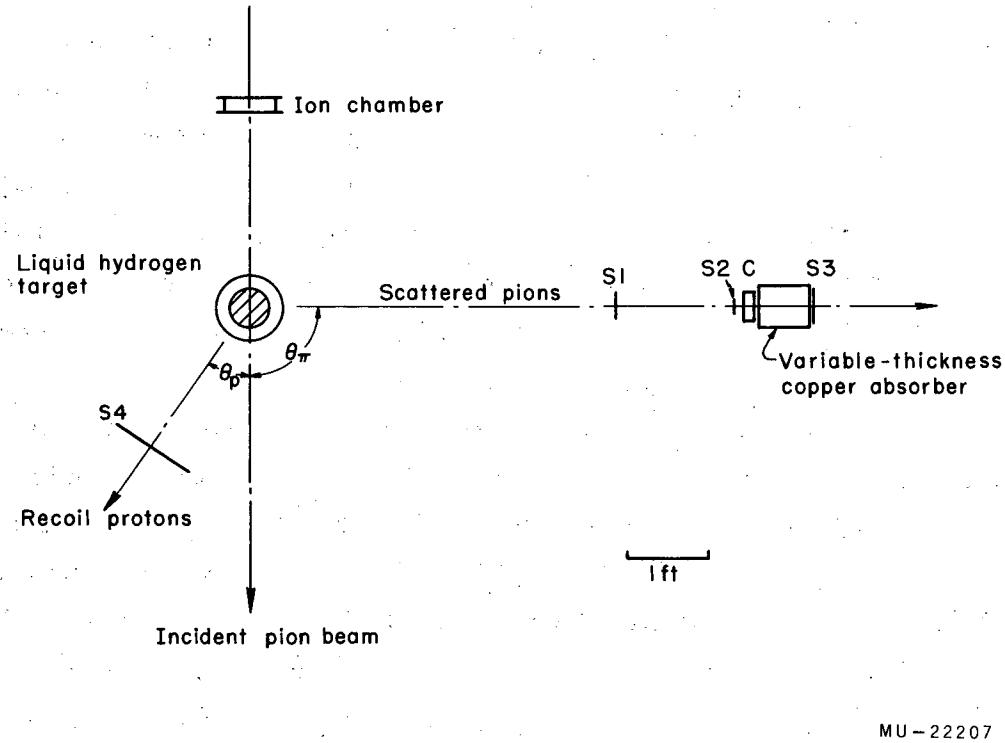

Fig. III-1. Scale drawing of the counter arrangements, including the hydrogen target used to measure the differential cross section.

Table III-I. Description of the components of the experimental apparatus indicated in Fig. II-1, III-1, IV-1, IV-3, and V-1, and described in the text.

Item	Designation	Description
Counters	S1	4-in. diam × 3/4-in. plastic scintillation counter
	S2	2-1/4-in. -diam × 5/8-in. thick plastic scintillation counter
	S3	5-in. -diam × 3/8-in. -thick plastic scintillation counter
	S4	12-in. -square × 1/2-in. -thick plastic scintillation counter
	S5	4-in. -diam × 1/4-in. -thick plastic scintillation counter
	S6	2-1/4-in. -diam × 1/4-in. -thick plastic scintillation counter
	S7	3-in. -diam × 1/4-in. -thick plastic scintillation counter
	S8	1.50-in. -diam × 1/8-in. -thick plastic scintillation counter
	S9	10-in. -diam × 1/2-in. -thick plastic scintillation counter
	C1	4-in. -square × 1-1/2-in. -thick water-filled Cerenkov counter
	C2	4-in. -diam × 72-in. -long SF_6-gas-filled Cerenkov counter
	IC No. 1	4-in. -diam × 2-in. long Argon-filled ionization chamber
	IC No. 2	7-in. -diam × 2-in. -long Argon-filled ionization chamber
Targets	T1	5-in. -diam × 19-in. -long polyethelene (CH_2) target
	T2	5-1/2-in. -diam × 8-in. -high liquid hydrogen target
	T3	6-in. -diam × 12-in. -long liquid hydrogen target
Magnets	Q1 and Q2	8-in. -diam 3-element quadrupole focusing magnets
	q1 and q2	4-in. -diam 3-element quadrupole focusing magnets

Magnets (con't)	M1	Deflecting magnet, 36×18-in. pole tips, 7-in. gap
	M2	Deflecting magnet, 36×18-in. pole tips, 8-in. gap
Absorbers and	A1	8-in. -square × 2-in. -thick carbon absorber
Collimators	A2	6-in. -square 80.17-g/cm^2 -thick copper absorber
	C	2-in. -square by 18-in. long lead collimator

of $\Omega = 0.855 \times 10^{-3}$ sr. The Cerenkov counter C1 had a threshold of $\beta = 0.75$. It rejected recoil protons and a large fraction of the very small number of inelastic pions (see Section V). S1 increased the angular definition of the telescope, thereby eliminating most of the background that was not target-derived. Counters S3 and S4 were used to search for possible systematic errors, as described later in this section. The apparatus used in run No. 2 was different only in that thinner counters S5 and S6 replaced S1 and S2.

The scattering angle θ was measured with the aid of a surveying transit, which was located in the center of the pion beam at a distance of 216.7 in. from the hydrogen target. To determine θ, both the distance between the transit and S2 and the angle between S2 and the hydrogen target (as seen by the transit) were measured. Either measurement fixes θ, but the two methods are complementary, since the former is more accurate for θ around 80 deg and the latter is better for forward and backward angles. The error in the angle measurements probably does not exceed 0.2 deg.

All counters were viewed by 6810-A photomultiplier tubes. The pulses from the Cerenkov counter C1 were amplified by a Hewlett-Packard 460-A wide-band amplifier. Pulses from all counters were fed into a multi-input coincidence circuit of the Garwin type.[18] Output pulses from the coincidence circuit were fed into conventional scaling units. The resolving time of the system was about 20×10^{-9} sec. The appropriate counter voltages and cable lengths were determined experimentally by optimizing the coincidence rate as a function of these variables. When properly set, the coincidence rate was independent of counter voltage and delay over a wide range in these quantities. At a few angles the cross section was measured at normal voltage, +100 volts, and -100 volts on all counters. All three values were found to agree.

Accidental coincidences were measured at several angles by delaying various counter pulses 52×10^{-9} sec (the separation in rf pulses of the 184-in. cyclotron). They were found to be negligible. The accidental rate, which was almost independent of whether the hydrogen target was full or empty, was about 0.5% of the scattered pion rate. At a few angles, the cross section was measured at full

cyclotron beam, 1/2 full beam, and 1/4 full beam, and it was found to be independent of beam level. The rest of the data were taken at a level of 1/2 full beam.

Some of the incident mesons were scattered into the counter telescope by the hydrogen container and the vacuum jacket. This background was measured by counting the number of pions scattered into the telescope when the hydrogen target was empty. The true scattering rate from the hydrogen was taken as the target-full rate minus the target-empty rate,

$$I(\theta)/I_0 = [I(\theta)/I_0]_{\text{full}} - [I(\theta)/I_0]_{\text{empty}}.$$

The target-empty rate was generally about 25% of the full rate, and for the most forward points it reached almost 50%. This effect was so large that a great deal of time and effort was spent to make sure that the background was subtracted correctly.

A powerful method for eliminating this background was to count the recoil proton in coincidence with the scattered pion. This proton comes off at a well-defined angle for elastic pion-proton scattering. Unfortunately, the recoil proton could be counted with confidence over only a small range of pion scattering angles, around 90 deg. For larger pion angles, the proton recoiled more forward, causing the proton counter S4 to be jammed by the incident pion beam. For smaller pion angles, the proton energy was reduced to the extent that some of the protons were stopped in the target and target walls. The important fact was that the recoil protons could be reliably counted in coincidence with the scattered pions at 88 deg, and the result verified the data obtained when only the pions were counted. In the latter case, the target-empty count was 25% of target-full count; and in the former it was about 3%, but the hydrogen effect (target-full minus target-empty) was the same in both cases. This result indicated that the background was subtracted reliably at this angle.

Range curves of the scattered pion beam were taken at three scattering angles for both target full and target empty. These curves were obtained by measuring the fourfold coincidence (S1, S2, S3, C1) per unit incident-pion beam as a function of absorber between C1 and

S3; see Fig. III-1. Figure III-2 shows the result for target empty and for "hydrogen effect" (target full minus target empty) at an angle of 141 deg. The results at 41 deg and 88 deg were similar. No systematic error was suggested by these range curves. The "hydrogen effect" curve behaved precisely as one would expect the curve to behave for pions elastically scattered from protons. The background appeared to be mainly pions: their energy was not well defined, because they had scattered from a complex nucleus. It is important to notice that the background rate decreased rather slowly with absorber thickness. This means it was not seriously affected by the presence or absence of hydrogen in the target.

Finally, the background subtraction was checked by artificially increasing the target-empty rate by placing thin aluminum foil at the target entrance and exit windows. Even when the empty rate was doubled, the measured full-minus-empty rate remained the same.

B. Corrections to the Data

There were many corrections to be made in the raw data in order to obtain the true cross section. The experiment was designed to keep these corrections small, so that their uncertainties introduced only small errors into the final results.

The counter telescope (S1, S2, C1) was not 100% efficient. A few pions scattered toward the defining counter S2 did not register a coincidence in the telescope. This was caused by an interaction in one of the counters that scattered the pion so that it did not pass through all three counters of the telescope. The counter telescope was, however, essentially 100% efficient in counting pions that were not scattered out of the telescope.

This efficiency varied with scattering angle, primarily because of the variation of pion energy with scattering angle. In this experiment the energy of the scattered pions varied between 295 Mev and 115 Mev. It would have been virtually impossible to measure this efficiency accurately, because it was impossible to construct a known flux of pions whose energy and spatial distributions matched those of the scattered pion beam. The efficiency was calculated by using published data on the interaction of pions with hydrogen and carbon.[8,19,20,21]

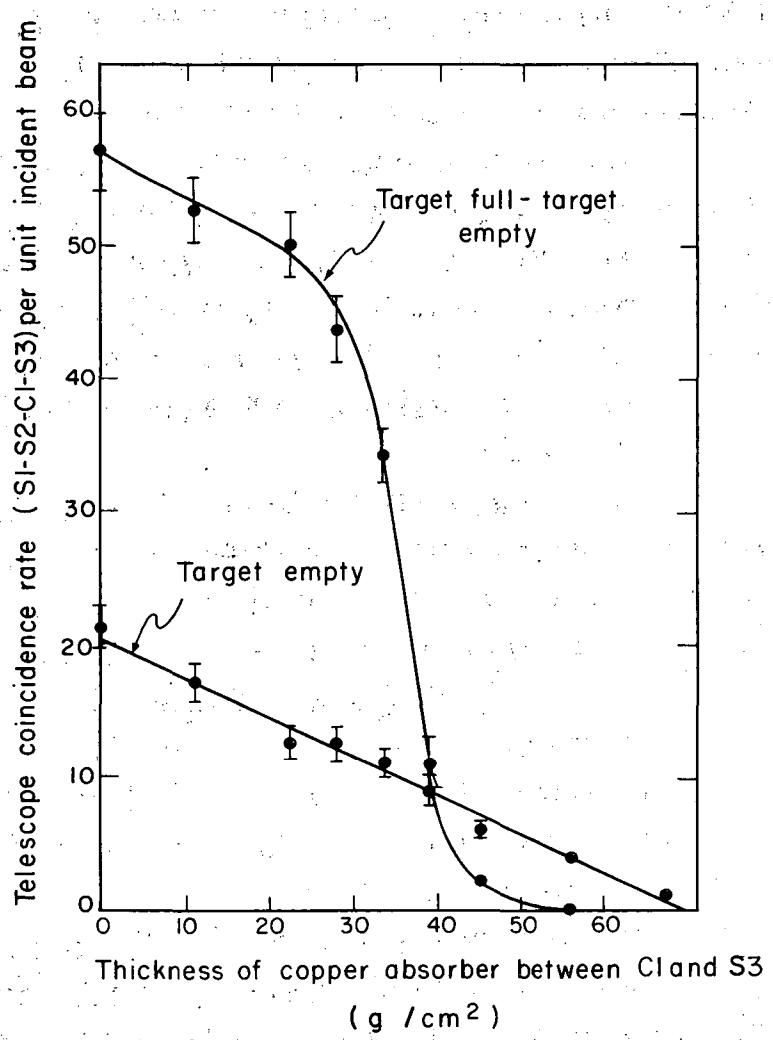

Fig. III-2. Range curve of the scattered pion beam at 141 deg, showing background (hydrogen target empty) and the "hydrogen effect" (target full-target empty).

This efficiency varied from 90 to 93.5% in run No. 1 and from 97 to 98.5% in run No. 2. The calculated values of the telescope efficiencies for run No. 1 (E1) and run No. 2 (E2) are plotted as functions of scattering angle in Fig. III-3. In the first run the major contribution to the inefficiency was the scattering of pions from the first counter S1. The calculation of this scattering was experimentally checked by fastening various thicknesses of additional plastic scintallator to counter S1, and observing the effect on the telescope coincidence rate. This was done at several scattering angles. The results confirmed the calculations. This method was reliable, since the actual scattered beam was used, but for the same reason the counting statistical errors were significantly large, i.e. about 1/3 the effect.

Some of the scattered pions undergo a second scattering before they are clear of the hydrogen target. This plural scattering distorts the angular distribution slightly, so that it was necessary to correct the data to remove this distortion. The correction is plotted as a function of scattering angle in Fig. III-3, and was obtained as follows. The total solid angle, as seen from the hydrogen target, was broken up into 144 sectors of $\Delta\theta$ = 15 deg and $\Delta\phi$ = 30 deg. The polar axis was taken in the direction of the incident pion beam, and ϕ = 90 deg was up. By use of data from this experiment, and neglecting the plural scattering correction as a first approximation, the number of pions scattering into each sector N_i' was calculated. The result was, of course, independent of ϕ. All particles scattering into a certain sector were assumed to have a single energy and direction, corresponding to the central value for that sector. Next, the probability for a scattered particle to be rescattered into the center of the i^{th} sector was calculated for all 144 choices of the first scattered direction. The contribution from all sectors was summed to give $N_{i,\,in}''$, which is the total number of pions scattered into the i^{th} sector via double scattering. Of course, it was necessary to use published data on positive pion-proton differential cross sections for pion energies of 100 to 300 Mev.[8, 20, 21] The energy of the first scattered beam depended only on the polar scattering angle, but the average amount of hydrogen traversed depended on ϕ. The number of pions that were originally scattered into the i^{th} sector and then scattered out again by a second scattering $N_{i,\,out}''$ was also computed. The quantity

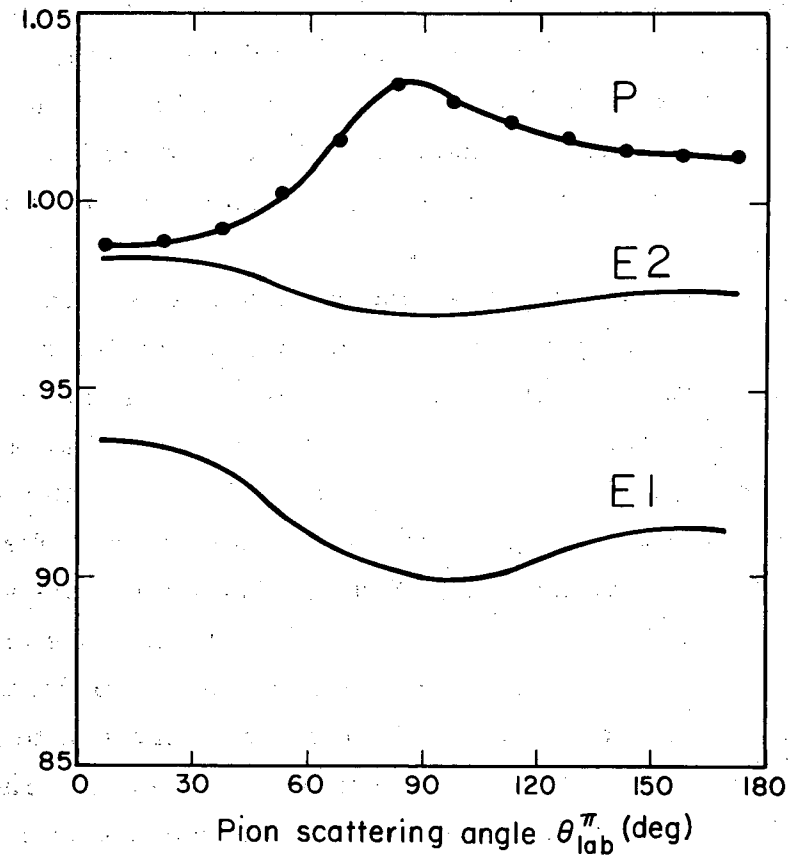

Fig. III-2. The corrections applied to the counter telescope coincidence rate $[I(\theta)/I_0]$ to compensate for plural scattering in the target, $P(\theta)$, and for the telescope efficiency in run No. 1, E1 (θ), and run No. 2, E2 (θ), as a function of pion scattering angle, θ. The corrections are given in the sense $[I(\theta)/I_0]_{measured} = E1(\theta)[I(\theta)/I_{0\ true}$, and similarly for E2 and P.

$P_i = (N_{i,\,in}'' - N_{i,\,out}'')/N_i'$ was computed for all sectors of $\phi = 0$. A smooth curve was drawn through the value of P obtained at these 12 angles. The telescope counting rate was corrected for double scattering by

$$[I(\theta)/I_0]_{measured} = P(\theta)[I(\theta)/I_0]_{true}.$$

The correction due to triple scattering was negligible.

About 10% of the scattered pions decay into muons before they are counted in the telescope. These muons generally continue in approximately the same direction and are counted in the telescope. There are two very small corrections to the data due to this decay. First, there is a correction much like the plural-scattering corrections, since the muon comes off at an angle with respect to the pion direction. This is calculated in much the same way as the plural scattering and is found to be negligible (less than 0.3%), because the difference between muon and pion direction is small (less than 8 deg). The second correction is in the efficiency of the telescope. The efficiency for counting muons is not the same as for pions. Muons do not suffer nuclear attenuation in the counters as do pions. The directional properties of the telescope discard a very few of the muons that pass through the telescope in a skew direction. When the efficiency curves are corrected for these effects the results are changed by less than 1%.

The angular resolution of this system was good. The rms spread in scattering angle due to finite counter and target sizes varied between 1.2 deg and 2.1 deg, depending on the scattering angle. The pion-beam divergence was 1.8 deg for beam No. 1 and 0.6 deg for beam No. 2. The data were corrected to account for this finite angular spread. However, this correction was significant only for scattering angles near 70 deg, where the curvature of the plot of the differential cross section vs scattering angle is large, and even here it amounted to less than 1%.

The Cerenkov counter C1 was not perfect in rejecting recoil protons; a few of these protons evidently produced enough scintillation light to register a coincidence. Fortunately, the range of protons recoiling at angles greater than 45 deg was not sufficient to pass out of the target and through the telescope to the last counter. Therefore, only the data at laboratory-system scattering angles less than 45 deg

had to be corrected for the proton contamination in the telescope coincidence rate. This proton contamination was measured by putting the big conjugate counter S3 in coincidence with the telescope at the appropriate angle to count the pions conjugate to the protons in the telescope. The contamination was found to vary between 1% and 1.5% (i.e., the Cerenkov counter was about 3% efficient in counting protons, and the ratio of pions to protons in this angular region varied from 3:1 to 2:1).

C. Results and Errors

The results of the measurements described in this section are given in Table III-II, and are plotted in the laboratory frame in Fig. III-4. At small angles the background increased rapidly as the scattering angle decreased. No data are reported for scattering angles less than 22 deg, where the target-empty rate was 1/2 target full, because the large subtraction may have introduced a significant error. Further results at smaller angles obtained with a more favorable arrangement are given in Table IV-1.

The errors associated with these measurements fall naturally into three classifications. First, the counting statistical errors, which are uncorrolated and presumably normally distributed. These errors are listed with the data points. The rms error in telescope counting rate for "hydrogen effect" was calculated as

$$\Delta[I(\theta)/I_0] = \{[I(\theta)/I_0{}^2]_{\text{full}} + [I(\theta)/I_0{}^2]_{\text{empty}}\}^{1/2}.$$

The second type of error is the error in the absolute cross-section scale, due to uncertainties in the number of protons in the target, the uncertainties in muon contamination, etc. The absolute-scale parameter ϵ was introduced to express this class of errors. The data are presented as $(1 + \epsilon)\,(d\sigma/d\Omega)$, where the same ϵ is common to all cross-section points, and the most likely value of ϵ is 0. The error in ϵ is estimated to be about 6%. This comes from the uncertainty in the absolute calibration of the ion chamber, 4%, and the uncertainty in the muon contamination, 3%. (This rather large error is assigned because the momentum-analyzed muon contamination was measured with a counter

Table III-II. Results of the differential cross-section measurements described in Section III. Additional data, between 10.0 deg and 32.0 deg (lab) are given in Table IV-I. The absolute normalization parameter, $\epsilon = 0.00 \pm 0.06$.

Pion laboratory-system scattering angle	Center-of-mass scattering angle	Differential cross section in the laboratory system	Differential cross section in the center-of-mass system	Run
θ^{π}_{lab} (deg)	θ_{cm} (deg)	$(1+\epsilon)(d\sigma/d\Omega)^{\pi}_{lab}$ (mb/ster)	$(1+\epsilon)(d\sigma/d\Omega)_{cm}$ (mb/ster)	
22.0	30.6	23.99± 0.63	12.94± 0.62	2
24.9	34.6	22.34± 0.51	12.28± 0.27	1
26.2	36.3	21.34± 0.64	11.84± 0.35	1
32.0	44.0	16.94± 0.17	9.82± 0.10	2
32.0	44.0	16.94± 0.19	9.82± 0.11	1
38.0	51.8	14.08± 0.42	8.59± 0.26	2
41.9	56.8	11.91± 0.46	7.54± 0.28	1
44.5	60.0	10.11± 0.22	6.58± 0.22	1
52.2	69.4	6.66± 0.15	4.71± 0.11	1
52.8	70.1	6.71± 0.24	4.78± 0.18	2
57.2	75.3	4.83± 0.12	3.62±0.09	1
62.7	81.6	3.466± 0.102	2.771±0.081	1
77.8	97.8	1.728± 0.076	1.663± 0.073	1
85.0	105.0	1.44± 0.06	1.51± 0.06	2
88.2	108.1	1.486± 0.059	1.623± 0.065	1
102.1	120.9	1.657± 0.061	2.083± 0.077	1
119.0	135.2	1.919± 0.093	2.934± 0.142	1
125.7	140.6	2.07± 0.08	3.36± 0.12	2
131.0	144.7	2.214± 0.086	3.76± 0.15	1
140.9	152.2	2.25± 0.11	4.10± 0.21	1
146.5	156.4	2.39± 0.09	4.51± 0.17	1
158.1	164.6	2.47± 0.09	4.91± 0.17	2
159.2	165.5	2.43± 0.09	4.85± 0.17	1

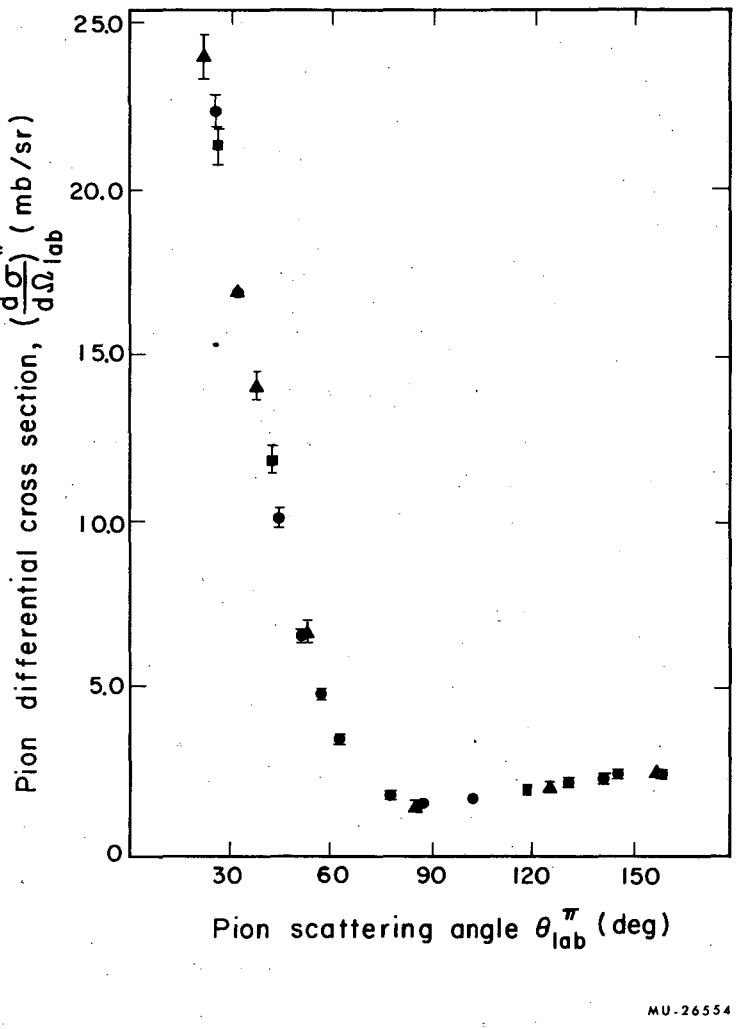

Fig. III-4. Differential cross-section data given in Table III-II plotted in the laboratory frame.

telescope, whereas the beam was monitored with an ion chamber with an area different from that of the defining counter of the telescope. If these muons had a spatial distribution at the second focus different from that of the pions, which is not unlikely, the muon contamination could have differed somewhat in the two cases.) There was also uncertainty in the number of protons in the target, 2% (due to uncertainty in the target size, the density of liquid hydrogen and possible error in folding in the beam profile); and uncertainty in the solid angle subtended by the counter telescope, 1%. Because of this rather large error in the absolute scale, one angle, $\theta^{\pi}_{lab} = 32$ deg, was measured with very small statistical counting errors (about 1%) in each run, including the small-angle data described in Section IV. The data from the different runs were then normalized to agree at this angle. The absolute values of the cross section at 32 deg differed by 3% between run No. 1 and run No. 2. This was as close as could be expected. The average value of the two runs was used to present the data in Table III-2.

The third class of errors were those associated with the various corrections that were made in the data. The uncertainty in the data resulting from errors of this type was small compared with the counting statistical errors.

The errors in the efficiency and the plural-scattering corrections are primarily due to the uncertainty in the cross-section data used in the calculations. This means that the deviation from unity in the efficiency curve has a fractional error of about ±20%. This leads to an absolute uncertainty of about 2% in the cross section. However, the relative efficiency at various angles is in error by less than 1%. The deviation from unity of the plural-scattering correction has a fractional error of about 45%. This relatively high error occurs because the plural-scattering correction is the difference between two terms, the number scattered in and the number scattered out.

The following equations were used to transform the data from the laboratory system to the center-of-mass system.

$$\text{Tan } \theta_{cm} = \frac{\sin \theta_{lab}}{\gamma_0 (\cos \theta_{lab} - \beta_0/\beta)} ;$$

$$(d\sigma/d\Omega)_{cm} = (d\sigma/d\Omega)_{lab}$$

$$[\gamma_0^2 (\cos \theta_{lab} - \beta_0/\beta)^3 / \cos^3 \theta_{cm} (1 - \beta_0/\beta \cos \theta_{lab})],$$

where β_0 is the velocity of the center-of-mass frame with respect to the lab frame, and is given in terms of the incident pion momentum P^{π}_{lab}, and the total relativistic energy E of the pion plus proton in the lab system as

$$\beta_0 = P^{\pi}_{lab} c/E = 0.30795 \text{ for this energy,}$$

$$\gamma_0 = (1/1 - \beta_0^2)^{1/2} = 1.0511.$$

IV. DIFFERENTIAL CROSS-SECTION MEASUREMENTS AT SMALL ANGLES

It was important that the differential cross section be measured at smaller angles (10 to 20 deg) in order to observe the interference between nuclear and Coulomb scattering, because, if the signs of all the phase shifts are reversed, the computed differential cross section is unchanged except in the region of small angles where nuclear and Coulomb scattering interfere. Hence, an analysis of data given in Table III-2 would determine only relative and not absolute signs for a given set of phase shifts. The absolute sign was determined by measuring the interference between the nuclear scattering and the Coulomb scattering, which was known to be repulsive in this case.

In principle, this sign ambiguity could be resolved by the polarization data, since the sign of the polarization is reversed when the signs of all phase shifts are reversed. In practice, it was better to establish the absolute sign of the phase shifts by measuring the differential cross section at small angles and use the polarization data to resolve the various other ambiguities.

This interference had been observed at 113 Mev by Orear, using the nuclear emulsion technique.[22] It had not been observed previously above the resonance or in a counter experiment, where high statistical accuracy could be obtained.

A. Experimental Arrangement

The experimental arrangement used in measuring the differential cross section at small angles was similar to that used at large angles, which was described in Section III. Some changes were necessary, however, and they are discussed in this section.

The pion spectrograph was altered to give a more suitable beam. A diagram of the modified magnet system, called pion spectrograph No. 2, is shown in Fig. IV-1. One significant change was that this beam was more nearly parallel than beam No. 1; the rms angle of divergence was 0.7 deg, compared with 1.9 deg for the first beam. This was accomplished by increasing the distance between the final quadrupole and the final focus, and by using smaller-aperture quadrupole magnets. This change was made

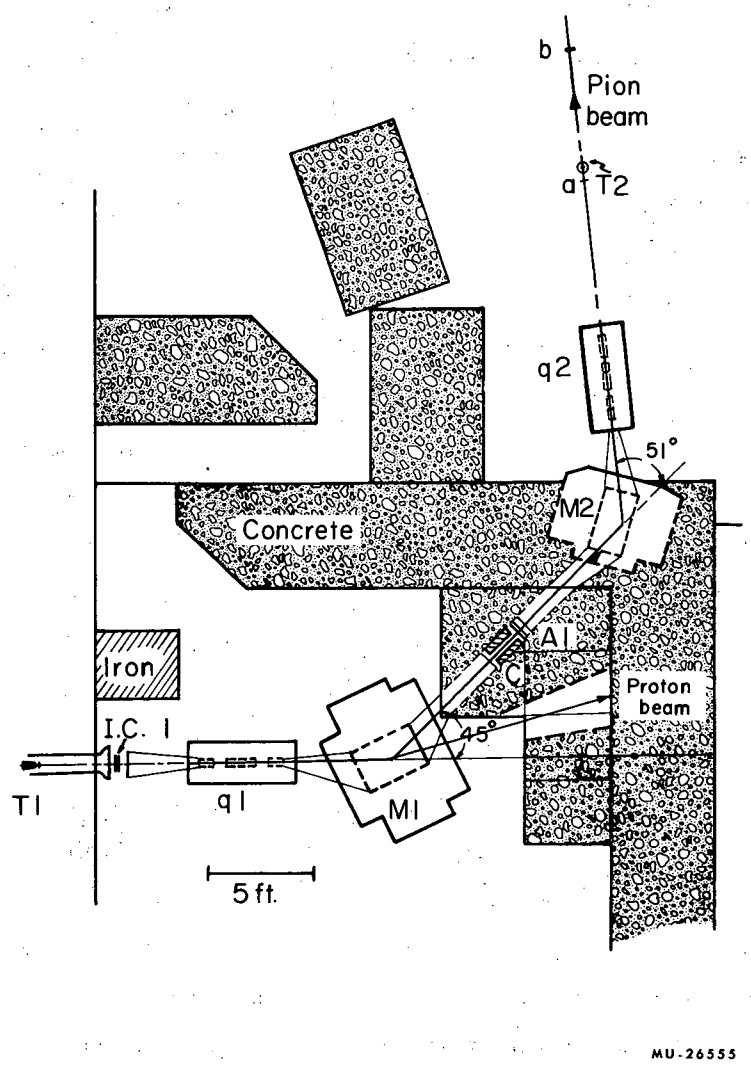

Fig. IV-1. Plan view of pion spectrograph No. 2. A description of the components is given in Table III-I.

so that the counter telescope could be brought in to smaller angles without encountering the incident beam. A plan view of the last quadrupole, the hydrogen target, and the telescope set at 10 deg is shown in Fig. IV-2. Note the lead wall which serves to hide the counter telescope from the exit aperture of the final quadrupole. This wall was essentially out of the incident beam, but it stopped that very small fraction of the incident pions which diverged sufficiently from the beam center line to pass through the telescope. Such stray particles were a very small fraction of the incident beam, but were comparable to the number of pions scattered into the telescope by the hydrogen target.

The cross-sectional area of this pion beam at the hydrogen target was reduced to 1/4 of that of the first beam. (Figure IV-3) This was accomplished by taking great care to minimize the size of the proton beam at T1, and by reducing the fractional momentum bite accepted by the magnet system from ±2.5% to ±1.0%. Reducing the momentum bite improves the final image, since "chromatic" aberration was the most important aberration in the magnet system. It was accomplished by using a small 2-in.-square collimator at the first focus in place of the field lens. This decrease in beam area was an important improvement, because it increased the fraction of the beam that passed through the thin windows on the hydrogen target, and therefore cut down target background. This scattering from the target walls, which was very strongly forward-peaked, presented the biggest obstacle to measuring the cross section at small angles. These improvements in beam size and divergence cost a factor of ten in intensity. However, this was not serious because the cross section was large in the forward direction, so that the counting rate stayed high.

The counter telescope was modified in one respect. The Cerenkov counter was replaced by a copper absorber, of thickness 80.17 g/cm^2, backed up by a scintillation counter (see Fig. IV-3). The absorber stopped recoil protons and inelastic pions. For small-angle work this telescope was somewhat superior to the one involving the Cerenkov counter for two reasons. First, it was less sensitive to background scattering from the target walls, since its threshold was higher. Second, it allowed a more correct treatment of the target-empty subtraction. This subtraction assumes that the background rate is independent of

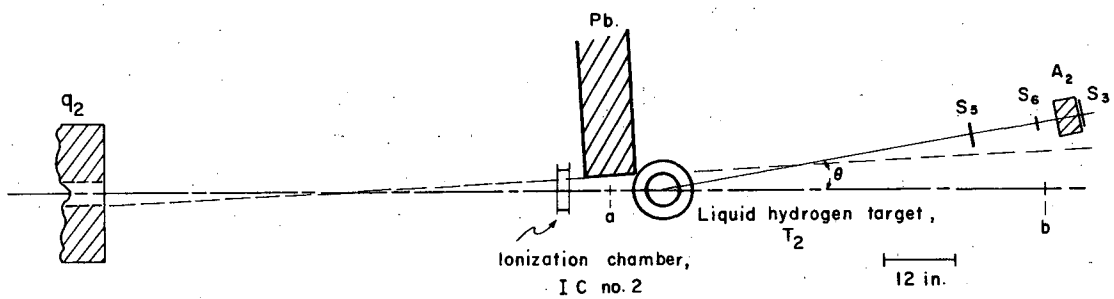

MU-26557

Fig. IV-3. Scale drawing of the hydrogen target and counter telescope (θ = 10 deg) used to measure the differential cross section in the region of Coulomb interference. A description of the components is given in Table III-I.

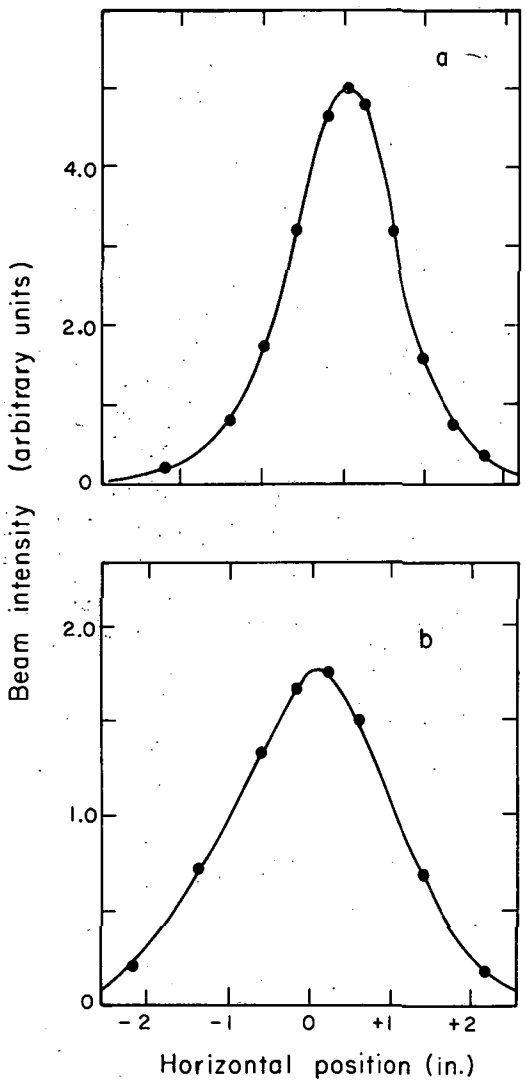

Fig. IV-2. Horizontal beam profile at positions a (9 in. up beam from T2) and b (66 in. down beam from T2). Full width at half maximum is 1.6 in. for a, 2.4 in. for b. The vertical profiles were somewhat sharper, having full width at half maximum equal to 1.4 in. and 2.3 in. at a and b respectively.

whether the target is full or empty. Let us consider the reasons why this may not be true. First, the background produced in the front of the target undergoes some scattering by the hydrogen. Second, the incident beam is attenuated by the presence of hydrogen in the target, so that less background is produced in the rear walls of the target when the target is full. Fortunately, these two effects were found to be small, because less than 3% of the pions interact in the target, the scattering was almost entirely elastic, and it was strongly forward-peaked. Hence, the amount of background produced in rear walls in essentially unchanged, and about as much of the background produced in the rear walls is scattered into the telescope as is scattered out by the presence of hydrogen in the target. There was a third effect, which was the degrading of background by the hydrogen. Some of the background that was just above the threshold of the telescope when the target was empty was slowed to below the threshold when the target was full. To compensate for this effect, the target-empty rate was taken in two ways: first, with the telescope exactly as when target-full data were taken, and second, with 2.29 g/cm^2 of copper added to the absorber, to compensate for the stopping power of the hydrogen. Neither of these measurements was correct. The first one ignored the degrading effect of the hydrogen, and thus gave a value of the background that was too large. The second measurement incorrectly assumed that all background was degraded by the hydrogen, and the extra absorber also scattered some pions out of the telescope, so it gave a value of the background that was too small. However, the measured background rate differed by only about 2.5% between these two methods, so that it was possible to use the average value without introducing significant error in the results.

There are strong objections to using a telescope of this type over the entire angular region, because it would be necessary to change the absorber thickness from several inches of copper to a small fraction of an inch as the scattering angle was varied. Hence, the telescope efficiency would vary drastically with scattering angle. It would be nearly impossible to measure this efficiency to better than 3 to 5% accuracy, so the data would be subject to a rather large systematic error. However, this telescope was used for scattering angles of only

10 deg to 32 deg. In this angular region, the energy of the scattered beam and the apparent target size were almost constant, so it was possible to use the same thickness of absorber at all angles and to assume that the telescope efficiency was constant throughout this angular region. This efficiency was determined by normalizing these data to those obtained with the high-efficiency telescope at 32 deg (see Section III), and was found to be 0.551±0.008. The efficiency was also calculated by using published data on pion cross sections in copper.[19,23] The calculated efficiency varied less than 0.5% between 10 deg and 32 deg. The calculated value of 0.518 agrees well enough with the measured value to indicate that the calculations have some validity. The cross section was also measured with both telescopes at 22 deg. The two measurements are found to agree, if the efficiency at 22 deg is assumed to be the same as that measured at 32 deg. Finally, the incident pion beam was sufficiently similar to the scattered beam at zero deg for the efficiency at zero deg to be measured by using the unscattered beam. The ratio S5, S6, S3/S5, S6 was measured. After corrections for attenuation in S5, for the muon contamination in the incident pion beam and for the fraction of scattered pions that decay into muons before reaching the telescope, an efficiency of 0.564±0.17 was obtained at zero deg. Thus, it is thought that the error introduced by assuming the efficiency constant between 10 deg and 32 deg was negligible.

The differential cross section was measured for both left and right scattering at all angles and found to agree. Accidental coincidences were negligible, and the cross section was found to be independent of both beam level and counter voltages.

B. Results and Errors

The data are given in Table IV-I. The errors quoted are statistical errors only and represent the standard deviation of the measurement. These data are plotted in Fig. IV-4, along with the predicted shape of the cross section for both constructive and destructive interference. These curves were predicted on the basis of the cross section data at c.m. scattering angles greater than 44 deg (Table III-2), by the method described in the Section VI. The uncertainty in either of these curves is small compared with the separation between the two.

Table IV-I. Results of the differential cross-section measurements at small angles. The errors given are standard deviations and are independent.

$$\epsilon = 0.00 \pm 0.06$$

θ^{π}_{lab}	θ_{cm}	$(1+\epsilon)(d\sigma/d\Omega)_{lab}$	$(1+\epsilon)(d\sigma/d\Omega)_{cm}$	$\frac{[I(\theta)/I_0]_{empty}}{[I(\theta)/I_0]_{full}}$
10.0	14.0	36.59±1.17	18.71±0.60	0.60
14.0	19.6	30.97±0.90	16.05±0.46	0.30
18.0	25.2	26.19±0.59	13.82±0.31	0.18
22.0	30.6	24.18±0.64	13.05±0.34	0.12
26.0	36.0	20.61±0.69	11.42±0.38	0.09
32.0	44.0	16.94±0.17	9.82±0.10	0.07

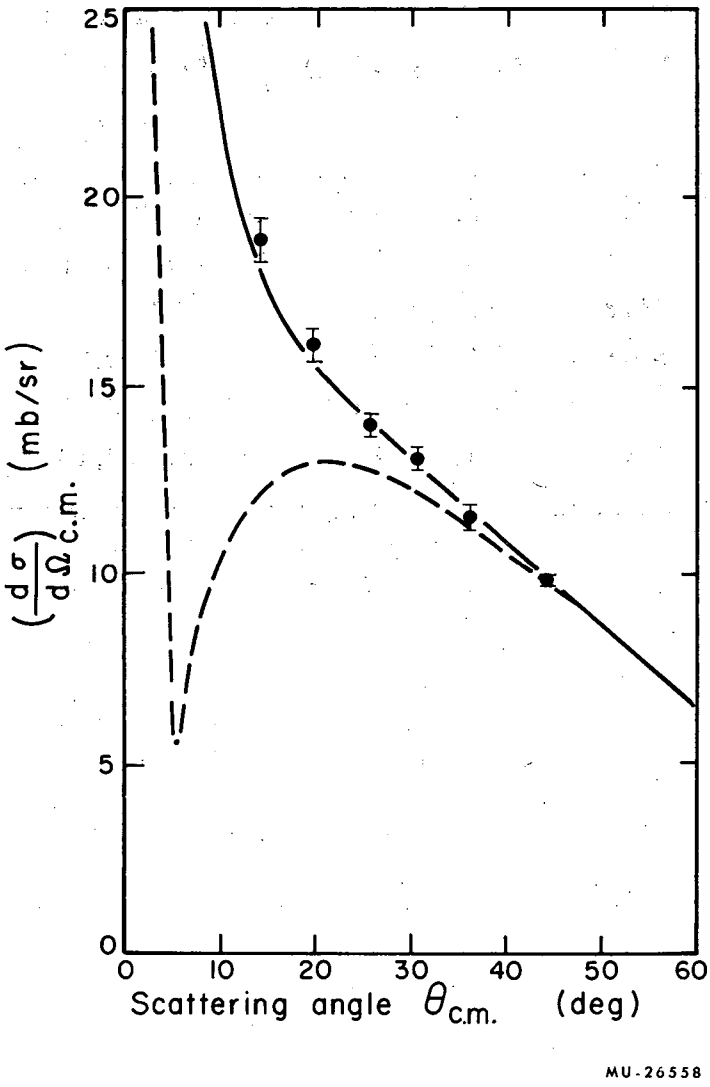

Fig. IV-4. Differential cross section in the region of the Coulomb interference. The experimental points are from Table IV-I. The two curves show the behavior predicted by the data for 44 deg to 165 deg (Table II-II) in the case of constructive interference (solid line) and destructive interference (dashed line).

The results are satisfactory. The data seem to rule out destructive interference between nuclear and Coulomb forces, and agree quite well with the cross section predicted under the assumption of constructive interference. Constructive interference is in agreement with the accepted description of low-energy pion-nucleon scattering. That is, that the cross section is dominated by the $P_{3,3}$ phase shift, which is positive and passes through 90 deg around 190 Mev.

There were two principal sources of possible systematic error. One of these was the assumption that the efficiency of the telescope was constant for scattering angles between 10 deg and 32 deg in the laboratory system. The other was the large target-empty subtraction at small angles. Both of these subjects were discussed in the preceding section, and the case was made that probable errors arising from these sources were smaller than the quoted statistical errors.

V. TOTAL CROSS-SECTION MEASUREMENT

The total cross section σ_T for 310-Mev pions on protons was measured by attenuation. The purpose of this measurement was to check the absolute scale factor ϵ of the differential cross-section data, and to reduce the uncertainty in this factor. In the approximation that elastic scattering is the only channel through which 310-Mev positive pions and protons interact, we have

$$\sigma_T(\theta_c) = 2\pi(1 + \epsilon) \int_{\theta_c}^{\theta_c'} \frac{d\sigma}{d\Omega}(\theta) \sin\theta \, d\theta,$$

where θ_c is the cutoff angle (see Fig. V-1); pions that scatter at an angle less than θ_c are detected in the back-up counter and appear as if no scattering had occurred. The upper limit on the integral is necessary because pions that are scattered at an angle greater than θ_c' produce protons that recoil at an angle less than θ_c. These protons are detected in the back-up counter, so here too the event appears as if no scattering had occurred.

The approximation that elastic scattering is the only interaction is not exactly true. Two other reactions are known to take place at this energy. They involve pion production:

$$\pi^+ + p \rightarrow \pi^+ + \pi^0 + p,$$

$$\pi + p \rightarrow \pi^+ + \pi^+ + n.$$

We are interested in the total inelastic cross section σ_I, which is the sum of the total cross sections for these two reactions. There are almost no experimental data on σ_I at 310 Mev. However, a reasonable estimate of the value can be made. Willis has measured $\sigma_I = 2.85 \pm .5$ mb, and the ratio $\sigma(\pi^+ + p \rightarrow \pi^+ + \pi^0 + p)/\sigma(\pi^+ + p \rightarrow \pi^+ + \pi^+ + n) = 1.5 + 1.5 - 0.5$ mb at 500 Mev.[24] In a theoretical paper, which uses experimental data on $\pi^- + p \rightarrow \pi^+ + \pi^0 + n$ at energies near 310 Mev, Rodberg predicts $\sigma_I(\pi^+ + p \rightarrow \pi^+ + \pi^0 + p) \approx 0.4$ mb at 310 Mev.[25] If we accept this value and assume Willis's ratio holds at 310 Mev, we have $\sigma_I \approx 0.6$ mb at 310 Mev. Theories of the energy dependence of σ_I, coupled with Willis's measurement at 500 Mev, predict $\sigma_I \approx 1/2$ mb at 310 Mev.[26,27]

Thus, a reasonable value of σ_I appears to be 0.5±.5 mb. Since the total elastic cross section is about 60 mb, the inelastic scattering is almost negligible.

A. Experimental Arrangement

The arrangement of the counters and the hydrogen target used to measure the total section is shown in Fig. V-1. A description of the counters is given in Table III-I. The second pion beam (described in Section IV) was used with the circulating beam of the cyclotron cut to approx 10^{-4} of maximum. The number of incident pions, I_0, was defined by the triple coincidence rate S7-C2-S8. The number of incident mesons that passed through the target unscattered, I, was given by the quadruple coincidence S7-C2-S8-S9. The position of S9 was varied to change the cutoff angle θ_c. Figure V-1 shows the two extreme positions of S9 corresponding to θ_c = 8.3 deg and 15.2 deg. The total cross section is given as

$$\sigma_T(\theta_c) = \frac{1}{N} \ell n \frac{I_0}{I} \frac{I'}{I_0'},$$

where primed quantities are the target-empty measurements, and the unprimed quantities are target-full data; N is the target thickness in protons/cm^2. The rms statistical counting error is

$$\Delta\sigma_T(\theta_c) = \frac{1}{N}\left(\frac{1}{I} - \frac{1}{I_0} + \frac{1}{I'} - \frac{1}{I_0'}\right)^{1/2}.$$

The total cross section was measured with two targets designated T2 and T3, which were 5.5 in. and 12 in. thick, respectively. Typically, $I/I_0 \approx 0.914$ and $I'/I_0' \approx 0.976$ for the long target, and $I'/I_0' \approx 0.948$ and $I/I_0 \approx 0.977$ for the short target.

The incident pion beam was corrected for muon and positron contamination, as described in Section II. The same number was subtracted from I as from I_0, as essentially all of the muon contamination passes through the target without scattering out. The fraction of the meson beam that was scattered out by multiple Coulomb scattering in counter S8 and the hydrogen target was negligible for this geometry.[14] The muons that come from pions that decayed between the beam-defining counter S8 and the back-up counter S9 passed through the back-up

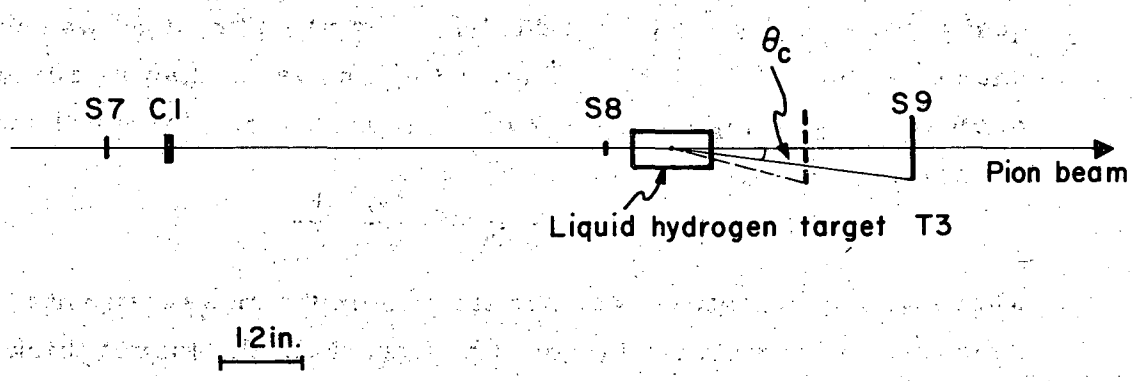

Fig. V-1. Scale drawing of the hydrogen target and counter arrangment used in the total cross-section measurement.

counter. Hence, these decays were not confused with scattering events. The cutoff angle was corrected to account for the finite target length. This correction amounted to about 1/2 deg. Accidental coincidences were completely negligible; cross-section measurements were made at normal beam level, 3 times normal, and 1/3 normal for θ_c = 10.5 deg. All these measurements agreed. Finally, the data at several angles were also taken with the coincidence circuits switched. The results were found to be independent of which circuit counted triples (I_0) and which circuit counted quadruple coincidences (I).

B. Results and Errors

The results of the total cross-section measurements are given in Table V-I, and are plotted in Fig. V-2. The errors listed are independent counting-statistical errors only. There is also a 2% error common to all points that arise from uncertainties in target thickness, muon contamination, and cutoff angle.

There are several items to note concerning the internal consistency of these results. First, the data from the two different targets agree quite well. Next, the variation of $\sigma_T(\theta_c)$ with θ_c agrees with the dependence predicted by the differential cross section (see Fig. V-2). Thus, if one uses these total cross-section data to compute the scale factor ϵ, the value obtained is independent of the cutoff angle chosen. The value of ϵ obtained from these data also agreed with the differential cross-section data. The value obtained from the total cross section was $\epsilon = -.018 \pm .025$, compared with the value $0.00 \pm .06$ given with the differential cross-section data in Table III-II. This total cross section also looks reasonable when compared to existing π^+-p total cross sections in this energy region.[28, 29, 30]

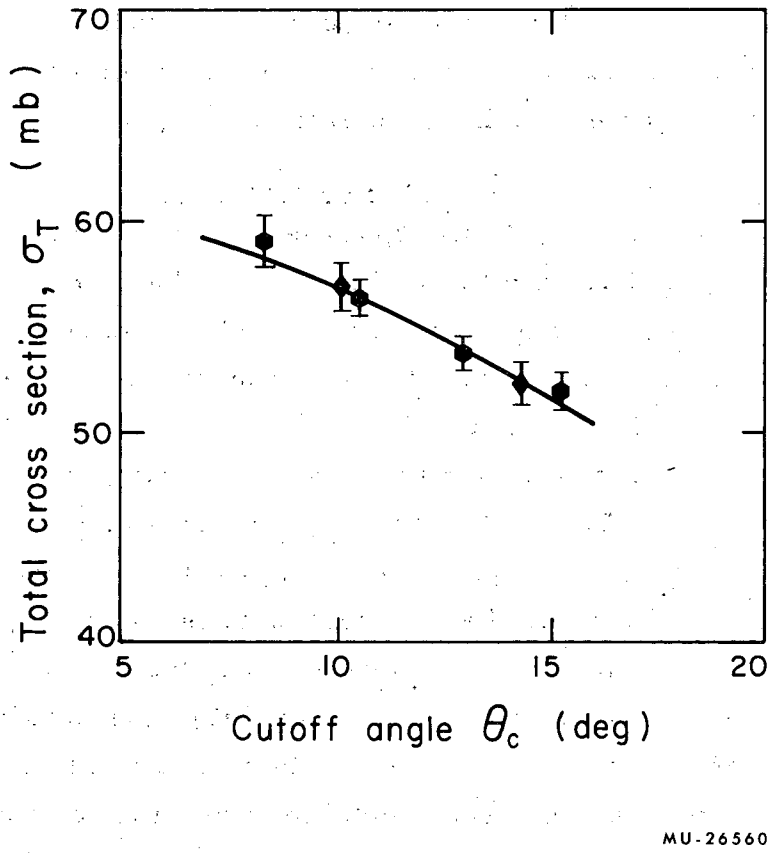

Fig. V-2. Total cross section of hydrogen for 310-Mev π^+ as a function of the cutoff angle θ_c. The experimental points are from Table V-I. The curve is the dependence predicted by the differential cross-section data when normalized to the point at 10.5 deg.

Table V-I. Results of the total cross-section measurements described in Section V. The errors listed are standard deviations and are due to counting statistics only. Each point also contains a 2% systematic error due primarily to uncertainty in target thickness, muon contamination, and cutoff angle.

Cutoff angle, θ_c (deg)	Total cross section, $\sigma(\theta_c)$ (mb)	Target number[a]
8.3	59.8± 1.2	T3
10.5	56.9± 0.8	T3
12.9	54.2± 0.8	T3
15.2	52.4± 0.8	T3
10.1	57.5± 1.0	T2
14.3	52.6± 1.0	T2

[a] Target T3 was 12 in. thick and Target T2 was 5.5 in. thick.

VI. THE PHASE SHIFT ANALYSIS

A. Search Program

A phase-shift analysis of these data was made with the aid of an IBM-709 computer. The computer made a least-square fit to the experimental data using the grid search method. It computed the usual quantity, $\chi^2 = \sum_i [(x_i^c - x_i^E)/E_i]^2$, where x_i^E is the experimental value of x_i, E_i is the experimental error, and x_i^c is the value of x_i calculated from a given set of phase shifts. The summation is over all experimental data. These data consist of the differential cross-section data given in Table VI-I, which is a summary of those given in Tables III-II and IV-I, the measurements of the polarization of the recoil proton that were made simultaneously with the cross-section measurements (Table VI-II),[31] and the value of the total cross section at $\theta_c = 10.5$ deg from Table V-I. Starting from a given set of phase shifts, the computer varied each phase shift by small increments until χ^2 was minimized. It cycled through all phase shifts several times until it reached a minimum χ^2 at which a small change in any phase shift caused χ^2 to increase. This minimum was not necessarily the absolute minimum, but only a depression in the hyperspace in which χ^2 is plotted as a function of the phase shifts. There may be several such minima. Which one the computer finds depends upon the set of phase shifts it starts from. In making our search, we started at several hundred different random sets of phase shifts in an effort to find all these minima.

In order to relate experimentally observable quantities with phase shifts, the non-spin-flip scattering amplitude $f(\theta)$, and the spin-flip amplitude $g(\theta)$ are expanded in terms of partial waves:[32]

$$f(\theta) = \lambda \sum_{\ell=0}^{\infty} \{(\ell+1) \exp(i\delta_\ell^+) \sin\delta_\ell^+ + \ell \exp(i\delta_\ell^-) \sin\delta_\ell^- \} P_\ell(\cos\theta)$$

$$g(\theta) = \lambda \sum_{\ell=1}^{\infty} \{\exp(i\delta_\ell^+) \sin\delta_\ell^+ - \exp(i\delta_\ell^-) \sin\delta_\ell^- \} P_\ell^1(\cos\theta)$$

where δ_ℓ^+ is the phase shift for the state $J = \ell \pm 1/2$, where ℓ denotes orbital angular momentum. The phase shifts are real quantities in the absence of inelastic scattering. The λ is the center-of-mass wave-

Table VI-I. Summary of the differential cross-section data given in Tables III-II and IV-I that were used in the phase-shift analysis. $\epsilon = 0.00 \pm 0.06$.

Center-of-mass scattering angle θ_{cm} (deg)	Differential cross section, $(1 + \epsilon)(d\sigma/d\Omega)^{\pi}_{cm}$ (mb/sr)
14.0	18.71±0.60
19.6	16.05±0.46
25.2	13.82±0.31
30.6	12.99±0.25
34.6	12.28±0.27
36.2	11.65±0.27
44.0	9.82±0.15
51.8	8.59±0.26
56.8	7.54±0.28
60.0	6.58±0.22
69.6	4.73±0.10
75.3	3.62±0.09
81.6	2.77±0.08
97.8	1.66±0.07
105.0	1.51±0.06
108.1	1.62±0.07
120.9	2.08±0.08
135.2	2.93±0.14
140.6	3.36±0.12
144.7	3.76±0.15
152.2	4.10±0.17
156.4	4.51±0.17
165.0	4.88±0.12

Table VI-II. Experimental measurements of the polarization P of the recoil proton. The sign of the polarization is positive when a preponderance of the protons have their spin pointing in the direction $P_i \times P_f$, where P_i and P_f are initial and final pion-momentum vectors.

Center-of-mass scattering angle, θ_{cm} (deg)	Polarization P of the recoil proton.
114.2	+0.044±.062
124.5	-0.164±.057
133.8	-0.155±.044
145.2	-0.162±.037

length (over 2π) of the pion; P_ℓ and P_ℓ^1 are associated Legendre polynomials of degree ℓ and order 0 and 1, respectively. The differential cross section $d\sigma/d\Omega$ and the polarization P of the recoil proton are expressed in terms of $f(\theta)$ and $g(\theta)$:

$$d\sigma/d\Omega = |f(\theta)|^2 + |g(\theta)|^2;$$

$$P = 2 \text{ Im } [g^*(\theta) f(\theta)] / [|f(\theta)|^2 + |g(\theta)|^2].$$

The polarization is taken in the direction of $P_i \times P_f$, where P_i and P_f are pion momentum vectors before and after scattering. The effects of Coulomb scattering were included in the analysis. The method used was essentially that of Stapp, Ypsilantis, and Metropolis.[33, 34]

B. Results and Errors

The first thing that was apparent from this analysis was that we could not adequately fit our data using only S and P waves ($\ell_{max} = 1$), but that the data could be fitted with S-, P-, and D-wave phase shifts ($\ell_{max} = 2$). We also found that there is only one set of S-, P-, and D-wave phase shifts that fit the data. Other solutions were found, but none had a χ^2 low enough to have more than a 2 or 3% chance of being a valid solution. Table VI-III lists the phase shifts and the χ^2 for the SPD solution (SPD-Fermi I), and the best SP fit (SP-Fermi). The large χ^2 of the SP-Fermi set indicates that it is a very poor fit to the data. Each solution is designated by a name designed to show the position that this solution takes with regard to the various ambiguities, e.g. Fermi or Yang. I and II refer to the D-wave ambiguity.[3] I indicates the type of solution for $D_{3,3} - D_{3,5} > 0$.

Figure VI-1 shows the cross-section data on the center-or-mass frame. The dotted line represents the SP-Fermi solution which does not fit the data adequately in the backward direction. The solid line represents the SPD-Fermi-I fit which does fit the data. Figure VI-2 shows the experimental polarization data and the calculated values from SP-Fermi and SPD-Fermi I. This clearly shows how poor the best SP fit is.

Besides resolving the ambiguities, the polarization data reduced the errors on the small phase shifts to 1/2 or 1/3 the values obtained

Table VI-III. Phase-shift solutions to 310-Mev π^+ - p scattering data when all data are included (differential cross-section data of Table VI-I, polarization data of Table VI-II, and the θ_c = 10.5 deg total cross-section measurement given in Table V-I).

Solution	Phase Shifts (deg)							χ^2	
	$S_{3,1}(a_3)$	$P_{3,1}(a_{31})$	$P_{3,3}(a_{33})$	$D_{3,3}$	$D_{3,5}$	$F_{3,5}$	$F_{3,7}$	found	expected
SP-Fermi	-22.3	-8.1	136.1	a	a	a	a	92	24
SPD-Fermi I	-18.5± 0.6	-4.7± 0.6	134.8± 0.6	1.9± 0.4	-4.0± 0.4	a	a	15.8	22
SPDF-Fermi I	-17.2± 2.6	-2.9± 4.0	135.0± 0.6	3.1± 2.6	-4.9± 2.1	0.5± 0.6	-0.6± 1.4	14.1	20
SPDF-Fermi II	-35.5± 0.7	-16.1± 0.7	151.4± 0.8	-11.4± 0.5	13.1± 0.5	-1.1± 0.5	-1.8± 0.3	18.3	20
SPDF-Minami-Yang I	123.1	-22.4	3.1	158.6	0.2	-2.8	-0.1	17.6	20
SPDF-Yang II	-32	142.2	160.4	17.8	-6.4	-1.7	-1.3	26.6	20

[a] Held at zero throughout the analysis.

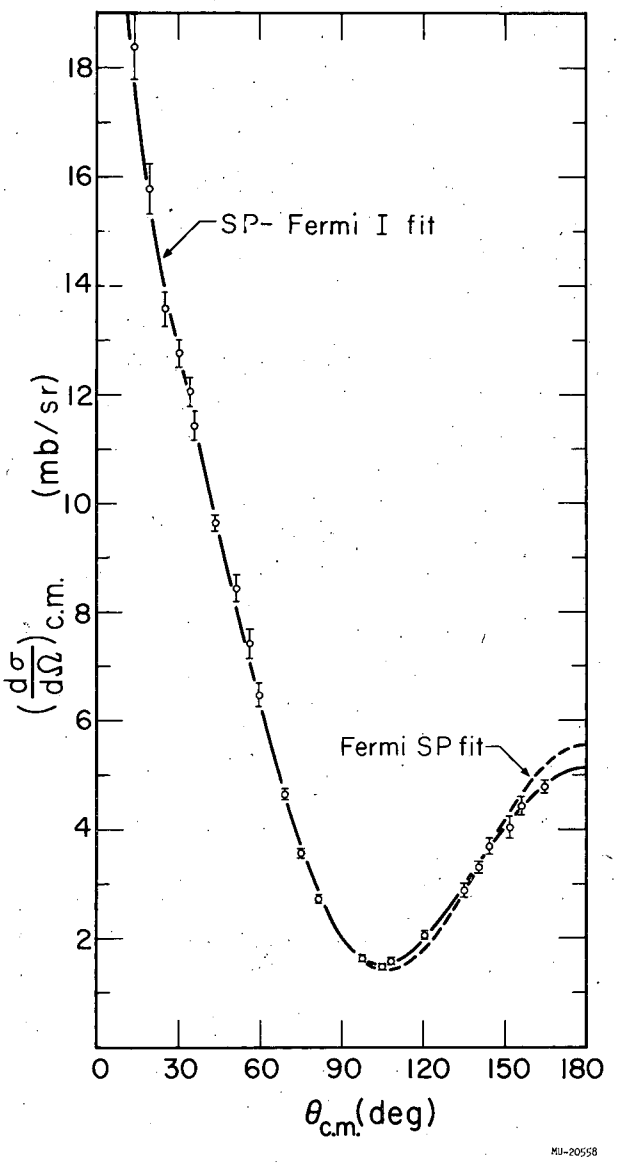

Fig. VI-1. The experimental differential cross-section data given in Table VI-I. The dashed line shows the cross section calculated from the SP-Fermi set of phase shifts given in Table VI-III. The solid curve corresponds to the SPD-Fermi-I set.

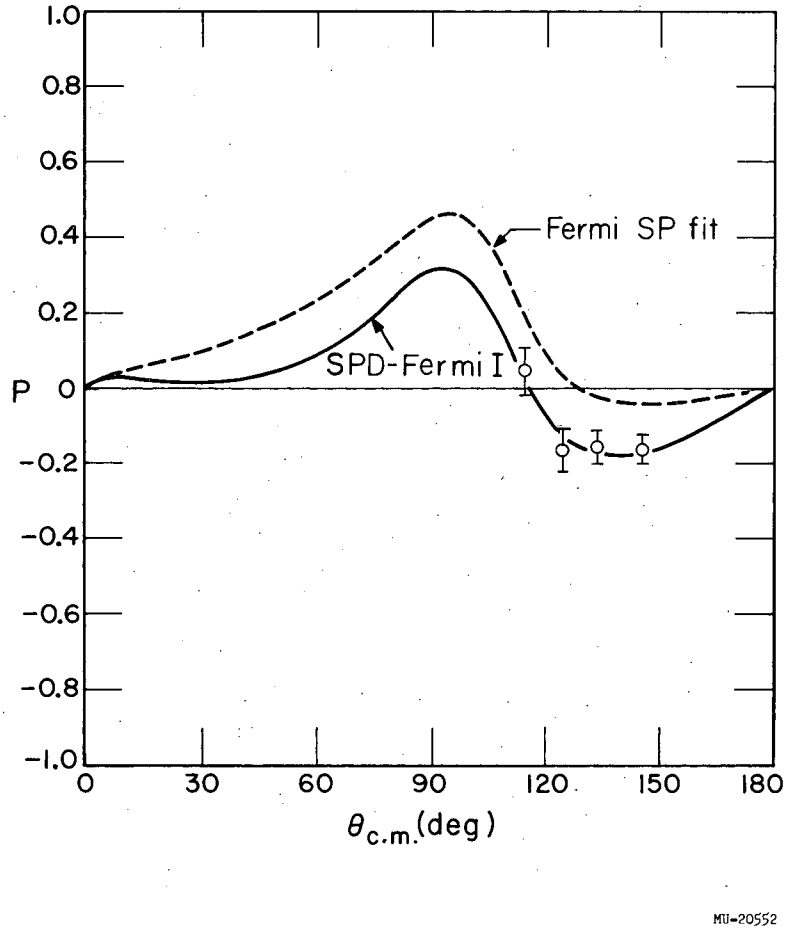

Fig. VI-2. The experimental recoil polarization data given in Table VI-II. The solid curve is obtained from the SPD-Fermi-I set of phase shifts and the dashed curve is from the SP-Fermi set (see Table VI-III).

when only our cross-section data were used in the analysis. These errors (from our cross-section data only) were, in turn, only 1/2 to 1/3 as large as errors in previous analyses.

At this point, the original goals seemed to have been reached. The S-, P-, and D-wave phase shifts were uniquely determined with very small errors purely on the basis of these experiments. These errors were, in fact, so small than an investigation of the effects of F waves was called for, as it was feared that their inclusion might well cause changes of greater than 0.4 degree in the D-wave phase shifts.

Two very surprising things happened when a search was made for SPDF solutions. As expected, the Fermi-I solution turned up with small F waves, approx 1/2 deg, and with the S-, P-, and D-wave phase shifts essentially unchanged from the SPD solution, but the errors on the phase shifts had increased by a factor of 5. These large errors are very disturbing! Secondly, those old ambiguities, which the polarization data had resolved in the SPD analysis, reappeared. F-wave phase shifts of only 1 and 2 deg allowed Fermi II to become a good fit to the data. Other types of solutions also became good fits to the data (Yang II and the Minami-Yang I). The solutions to the SPDF analysis are also given in Table VI-III. We certainly no longer have a unique set of phase shifts if the data are analyzed in SPDF waves. The data were not fitted significantly better when F waves were allowed to be nonzero, but this is to be expected because the SPD fit was already very good. Even though we reject the two Yang-type SPDF solutions for the usual reason (Yang-type solutions do not seem to agree with dispersion relations),[6] we are left with two Fermi-type SPDF solutions. We have two Fermi solutions because we are unable to resolve the D-wave ambiguity if F-wave phase shifts are allowed to be nonzero. It is worth noting that the phase shifts of the SPDF-Fermi I solution are strongly correlated. That is to say, fixing the value of one of them substantially reduces the uncertainty in the rest, or the phase shifts can change substantially while remaining a reasonably good fit to the data if they change in a certain way. For example, SPDF-Fermi-I can be distorted to a point where $S_{3,1} = -21.0$, $P_{3,1} = -10.2$, $D_{3,3} = -3.0$ and $D_{3,5} = +1.0$ with an M value still only 18.6.

VII. DISCUSSION OF RESULTS

This investigation indicates that it is difficult to obtain a meaningful set of phase shifts by using this method of analysis. It is very depressing to see that, by allowing small F-wave phase shifts (1 or 2 deg), we have introduced a new solution (Fermi II), which differs by 13° to 18° in S-, P-, and D-wave phase shifts from the original Fermi-I solution. This is precisely the kind of thing that we had assumed would not happen. We know of no a priori reason to limit the values of the F-wave phase shifts to less than those obtained in the SPDF solutions given in Table VI-3. Therefore, these SPDF sets must be considered as legitimate solutions.

We have not found a valid reason for discarding either of the two Fermi-type SPDF solutions. The D-wave phase shifts of the Fermi-I solution seem to show some agreement with the values predicted by Chew, Low, Goldberger, and Nambu from dispersion relations ($D_{3,3} = +0.3$, $D_{3,5} = -2.5$ deg at 310 Mev).[35] However, these predictions do not include the effect of the pion-pion interaction. We had hoped to determine the D-wave phase shifts accurately enough to obtain some information about the pion-pion interaction by comparing the experimental phase shifts with the predicted values of Chew et al., but we have not yet reached this point.

It seems that we are unable to determine accurately even the larger phase shifts at this time, although ours are the most extensive and most accurate π^{+}-p scattering data available. At this time, there does not appear to be any theoretical method of simplifying the analysis. However, this kind of help may appear in the future.

There is some reason to hope that these difficulties can be cleared up purely on the basis of the experimental data. The fact that we have four SPDF solutions instead of one is probably due to the very limited angular region of our polarization data. Figure VII-1 shows the behavior of P vs θ predicted by the various SPDF solutions. As expected, they differ violently at angles at which no experimental data tie them down. One or two measurements in this region may well result in a unique SPDF solution, depending, of course, on where these additional points fall. It is even possible that if enough points were measured so that P were well determined as a function of scattering angle a meaningful SPDFG fit could be obtained. We hope that after including polarization

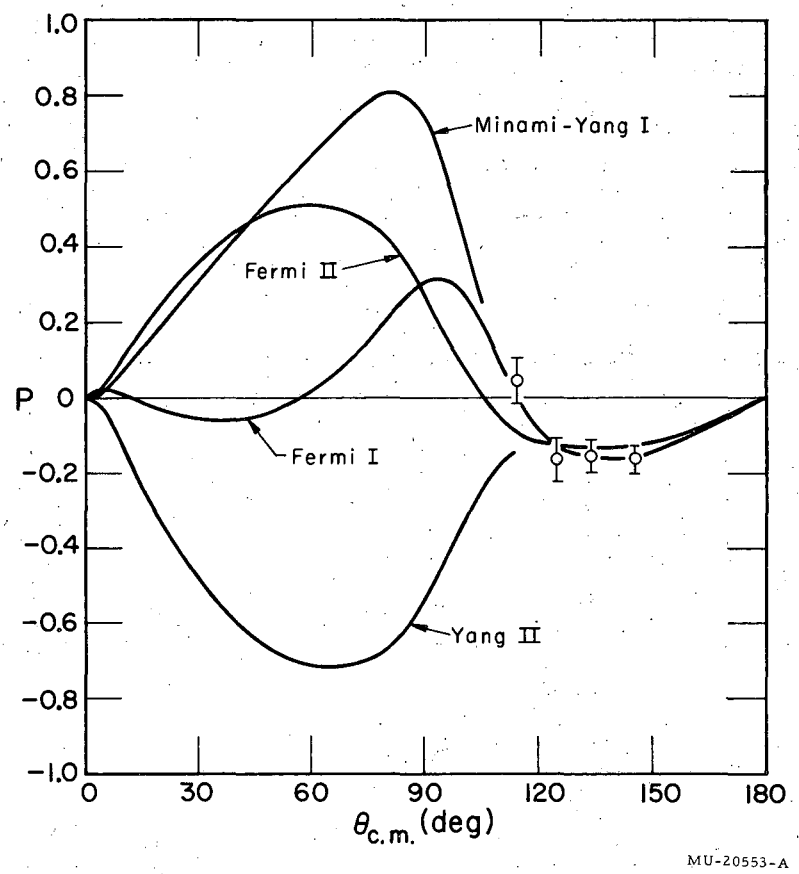

Fig. VII-1. Variation of the polarization with scattering angle predicted by the four SPDF solutions given in Table VI-III. The experimental data are also shown.

data taken over a wide angular region, one may still obtain an adequate fit to the data by using only a few phase shifts ($\ell_{max} = 2$ or 3), and that the results of the analysis will remain essentially unchanged when ℓ_{max} is increased by one. Although it has been impossible to measure the polarization P for $\theta_{cm} < 114$ deg, it does not seem unlikely that these data may be obtained in the near future. For instance, a helium analyzing target could be used in place of the carbon target to analyze the polarization of low-energy protons. The counting rate would be the problem here, because this helium analyzer would be less efficient by an order of magnitude than the carbon analyzer which gave approx 1 count/min for 10^6 pions incident per sec. Another method would involve starting with a partially polarized hydrogen target. Then a measurement of the azimuthal asymmetry in the differential cross section for scattering from this target would yield $P \cdot P_T$, where P_T is the polarization of the target. There is no inherent limitation to the angles at which P could be measured by this method; however, no such target is available at present.

Another way of attacking this difficulty might be to repeat these same experiments at other scattering energies. With data at several energies one might use dispersion relations to rule out some sets. Dispersion relations relate the real part of a scattering amplitude to an integral over the imaginary part as a function of energy, and thus restrict the energy dependence of a possible set of phase shifts. The most familiar dispersion relation deals with the forward scattering amplitude. In this case the imaginary part is related to the total cross section by

$$\text{Im } f(0) = \sigma_T/4\pi\lambda.$$

The energy dependence of the total cross section is reasonably well known, therefore the integral, and thus a prediction of the real part of the forward scattering amplitude, can be made. This is of very little use, however, because all the various sets of phase shifts given in Table VI-III yield the same value of the real part of the forward scattering amplitude, namely Re $f(0) = -0.686 \pm .012$ in units of the pion Compton wave length $\hbar/\mu c$. This value is, incidentally, in good agreement with the predicted values.[36, 37] The reason that all the phase shift solutions give the same value of Re f(0) is that it has a physical significance in

terms of the cross section,

$$\text{Re } f(0) = \{ [d\sigma/d\Omega\,(0)] - [\sigma_T/4\pi\lambda]^2 \}^{1/2}.$$

Thus it is essentially fixed by the differential-cross-section data.

Another dispersion relation that has received some attention deals with the forward spin-flip amplitude g(0). This is, of course, identically zero, therefore one uses the quantity $[d\, g(\theta)/d \sin\theta]_{\theta=0}$, which is nonzero. Davidon and Goldberger have employed the dispersion relation of this quantity in an attempt to show that the Fermi type of solution is favored over the Yang type. In this case neither the real nor the imaginary part has any simple physical interpretation. This is likely to be a good test of the phase shifts, however, it is very difficult to apply, because one must know the phase shifts as a function of energy in order to carry out the integral. Therefore data at other energies that are comparable to these results at 310 Mev are needed to make use of the dispersion relation for the spin-flip forward-scattering amplitude.

This was intended to be a decisive experiment, but it seems to have merely extended the horizon into a region of new difficulties; however, it is hoped that this work has been a significant step in the study of pion-nucleon scattering.

ACKNOWLEDGMENTS

The advice and council provided by Professor Emilio Segrè throughout several years of graduate study have been very valuable to the author. The experiments and the analysis benefitted greatly from the critical attention of Professor Owen Chamberlain. A few suggestions by Dr. Clyde Wiegand on experimental procedure proved extremely valuable. The author is indebted to Professor Tom Ypsilantis, Prof. Herbert Steiner, and Dr. Norman Booth for many enlightening discussions.

This program was carried out in collaboration with Dr. James H. Foote, who was chiefly responsible for the polarization data, and whose tireless effort in assembling the search program is greatly appreciated. Thanks are due to William B. Johnson and Olav T. Vik for contributing many useful suggestions and a great deal of hard work during these experiments.

The help and cooperation of Mr. James T. Vale and the cyclotron crew is greatly appreciated. Thanks are also due to the computer center, which is supervised by Mr. Kent K. Curtis.

This work was done under the auspices of the U. S. Atomic Energy Commission.

REFERENCES

1. E. Fermi, Phys. Rev. 91, 947 (1953).
2. H. A. Bethe and F. de Hoffmann, Mesons and Fields (Row, Peterson, and Company, Evanston, Illinois, 1955), Vol. II, p. 70 through 75.
3. E. Clementel and C. Villi, Nuovo cimento 5, 1343 (1957).
4. Shigeo Minami, Progr. Theoret. Phys. (Kyoto) 11, 213 (1954).
5. S. J. Lindenbaum and R. M. Sternheimer, Phys. Rev. 110, 1174 (1958).
6. W. C. Davidon and M. L. Goldberger, Phys. Rev. 104, 1119 (1956).
7. J. Orear, Phys. Rev. 96, 1417 (1954).
8. A. I. Mukhin, E. B. Ozerov, and B. Pontecorvo, Soviet Phys. JETP 4, 237 (1957).
9. M. G. Meshceriakov, B. S. Neganov, I. K. Vzorov, V. P. Zrelov, and A. F. Shabudin, "Magnetic Analysis of the Reactions $pp \rightarrow np\pi^+$ (1), $pp \rightarrow pp\pi^0$ (2), and $pp \rightarrow d\pi^+$ (3) at an Energy of 660 Mev," from Proceedings of the CERN Symposium on High-Energy Accelerators and Pion Physics, Vol. II (CERN, Geneva, 1956), p. 353.
10. M. G. Meshcheriakov, I. K. Vzorov, V. P. Zrelov, B. S. Neganov, and A. R. Shabudin, "Charged Pion Production by 660-Mev Protons on Beryllium and Carbon," from Proceedings of the CERN Symposium on High-Energy Accelerators and Pion Physics, Vol II (CERN, Geneva, 1956), p. 357.
11. N. E. Booth, O. Chamberlain, and E. H. Rogers, Nuovo cimento 19, 853 (1961).
12. O. Chamberlain, E. Segrè, and C. Wiegand, Phys. Rev. 83, 923 (1951).
13. Marvin Rich and Richard Madey, Range-Energy Tables, UCRL-2301, March, 1954.
14. R. M. Sternheimer, Rev. Sci. Instr. 25, 1070 (1954).
15. J. H. Atkinson and V. Perez-Mendez, Rev. Sci. Instr. 30, 865 (1959).
16. Robert R. Wilson, Phys. Rev. 86, 261 (1952).
17. D. B. Chelton and D. B. Mann, Cryogenic Data Book, UCRL-3421, May 15, 1956.
18. R. L. Garwin, Rev. Sci. Instr. 21, 569 (1950).

19. R. M. Sternheimer, Phys. Rev., 101, 384 (1956).

20. J. Ashkin, J. P. Blaser, F. Feiner, and M. O. Stern, Phys. Rev. 101, 1149 (1956).

21. G. Ferrari, L. Ferretti, R. Gessaroli, E. Manaresi, G. Puppi, G. Quareni, A. Ranzi, and A. Stanghellini, "Experimental Results on π^+-p Scattering in the Energy Range Between 70 and 130 Mev," from Proceedings of the CERN Symposium on High-Energy Accelerators and Pion Physics, Vol. II, (CERN, Geneva, 1956), p. 230.

22. J. Orear, Phys. Rev. 96, 1417 (1954).

23. S. J. Lindenbaum, Collisions of $\lesssim$ 1-Bev Particles (Excluding Electrons and Photons) with Nuclei, Ann. Rev. Nuclear Sci., 7, 317 (1957).

24. William J. Willis, Phys. Rev. 116, 753 (1959).

25. Leonard S. Rodberg, Phys. Rev. Letters 3, 58 (1959).

26. Jerrold Franklin, Phys. Rev. 105, 1101 (1957).

27. Emil Kazes, Phys. Rev. 107, 1131 (1957).

28. J. C. Brisson, J. Detoef, P. Falk-Vairant, L. van Rossun, G. Valladas, and Luke C. L. Yuan, Phys. Rev. Letters 3, 561 (1959).

29. A. E. Ignatenko, A. I. Muhkin, E. B. Ozerov, B. M. Pontecorvo, Soviet Phys. 3, 10 (1956).

30. S. J. Lindenbaum, Luke C. L. Yuan, Phys. Rev. 100, 306 (1955).

31. Owen Chamberlain, James H. Foote, Ernest H. Rogers, Herbert M. Steiner, Clyde E. Wiegand, and Thomas Ypsilantis, Phys. Rev. 122, 948 (1961).

32. J. Ashkin, Suppl. Nuovo cimento 14, 221 (1959).

33. H. P. Stapp, T. J. Ypsilantis, and N. Metropolis, Phys. Rev. 105, 302 (1957).

34. James H. Foote, Owen Chamberlain, Ernest H. Rogers, and Herbert M. Steiner, Phys. Rev. 122, 959 (1961).

35. G. F. Chew, M. L. Goldberger, F. E. Low, and Y. Nambu, Phys. Rev. 106, 1337 (1957).

36. T. D. Spearman, Nuovo cimento 15, 147 (1960).

37. James W. Cronin, Phys. Rev. 118, 824 (1960).